Remote Sensing of Environment 301 (2024) 113956

Contents lists available at ScienceDirect

Remote Sensing of Environment

journal homepage: www.elsevier.com/locate/rse

A rapid high-resolution multi-sensory urban flood mapping framework via DEM upscaling

Weikai Tan [a], Nannan Qin [b], Ying Zhang [c,*], Heather McGrath [c], Maxim Fortin [c], Jonathan Li [a,d,**]

[a] Department of Geography and Environmental Management, University of Waterloo, Waterloo, N2L 3G1, Ontario, Canada
[b] School of Remote Sensing and Geomatics Engineering, Nanjing University of Information Science and Technology, Nanjing, 210044, JiangSu, China
[c] Canada Centre for Mapping and Earth Observation, Natural Resources Canada, Ottawa, K1S 5K2, Ontario, Canada
[d] Department of Systems Design Engineering, University of Waterloo, Waterloo, N2L 3G1, Ontario, Canada

ARTICLE INFO

Edited by Menghua Wang

Keywords:
Urban flood mapping
Image fusion
Digital elevation model
Deep learning

ABSTRACT

Urban floods can cause severe loss of economic and social assets, and remote sensing has been an effective tool for flood mapping during disaster response. Due to the complexity of high-density urban structures, high-resolution (HR) optical images can only extract visible floods in open spaces, and floods in shadows and under the canopy are challenging to map. Accurate digital elevation models (DEMs) are essential for inundation estimation towards urban flood mapping, but HR DEMs are often unavailable due to the high acquisition costs. Through DEM upscaling, HR DEMs could be obtained from existing low-resolution (LR) DEMs using deep learning. To this end, a novel multi-sensory HR urban flood mapping framework is proposed in this research. The framework consists of three components: 1) a new DEM upscaling network to infer HR DEMs from existing LR DEMs with a fusion approach, 2) a rapid flood segmentation network to extract visible flood from very-high-resolution (VHR) optical images with limited human labelling, and 3) an accurate Geographical Information System (GIS)-based tool for floodwater extent and depth estimation from the visible flood information along with HR DEMs. The proposed framework was validated on a fluvial flood that occurred in Calgary, Canada, in 2013, where the proposed DEM upscaling network produced an upscaled HR DEM at 2 m resolution from an existing LR DEM at 18 m resolution. In addition, the proposed flood segmentation network has shown accurate visible flood extraction from VHR RGB aerial imagery with over 80% intersection-over-union (IoU) using 10% of human labelling as training samples. Finally, the floodwater extent and floodwater depth estimation using the proposed GIS tool showed significant improvement over conventional flood mapping methods.

1. Introduction

1.1. Backgrounds

Urban floods can cause severe loss of economic and social assets in urban regions due to the high density of population and infrastructure. The ubiquitous impervious surfaces in urban regions increase the runoff coefficient and peak discharge compared with natural land covers (Gyamfi et al., 2016). As a result, when water flows exceed the drainage capacity, water surcharge would spread across the surface flow networks, including roads, small watercourses and footpaths (Maksimović et al., 2009). Climate change may cause more rapid glacier melts and more extreme weather events, including heavy rainfalls, which poses new challenges to urban flood risk analysis (IPCC, 2014). The stakeholders and policymakers need accurate flood risk analysis models and maps to develop flood mitigation infrastructure and establish contingency plans (Merz et al., 2010).

Flood extent mapping during flood events is essential for disaster response and management, but rapid and effective inundation mapping is challenging in urban regions. Typical near real-time flood mapping is usually performed with medium-resolution (10–30 m) satellite optical images or synthetic aperture radar (SAR) images (Tanguy et al., 2017). However, medium-resolution optical images such as Landsat or Sentinel-2 do not provide enough resolution in dense urban areas, and SAR images usually suffer from the complicated structure of urban structures. There are high-resolution (HR) (below 5 m) optical satellite sensors such as SPOT and WorldView, but the timely acquisition is not often available during flood events due to weather conditions. Pluvial and fluvial floods often occur during springtime or heavy precipitation

* Corresponding author.
** Corresponding author at: Department of Geography and Environmental Management, University of Waterloo, Waterloo, N2L 3G1, Ontario, Canada.
E-mail addresses: ying.zhang@NRCan-RNCan.gc.ca (Y. Zhang), junli@uwaterloo.ca (J. Li).

https://doi.org/10.1016/j.rse.2023.113956
Received 29 September 2023; Received in revised form 3 December 2023; Accepted 10 December 2023
Available online 21 December 2023

events, so that cloud coverage would be challenging for HR imaging satellites to acquire clear imagery for real-time flood mapping (Huang et al., 2018). As a result, the more flexible airplanes and unmanned aerial vehicle (UAV) sensors are more suitable for real-time flood mapping and disaster response to provide accurate visible floodwater extent at sub-metre resolution (Feng et al., 2015; Zhang et al., 2019).

The real-time HR optical images can capture more details and have advantages in flood mapping due to the high spatial resolution. However, the optical images can only provide information from the sensor's view above the top layer, and limited information on the ground could be captured due to the occlusion of buildings and canopies. Optical images can only identify floodwater in open areas, and flood in shadows or under vegetation canopies is difficult to extract directly. As a result, accurate HR digital elevation models (DEMs) are necessary in addition to optical images for flood extent mapping and inundation models for urban flood risk analysis (Dottori et al., 2013). In this article, DEM refers to the elevation surface of bare earth, not including buildings and trees. Airborne Light Detection and Ranging (LiDAR) is the preferred source for HR DEM due to the high accuracy and the direct measurement of distance (Qin et al., 2023a), and hydraulic models can be applied to produce HR flood maps if the floodwater level can be determined (Muhadi et al., 2020). Visible floodwater extent extracted from real-time optical imagery could be used as a guide for inundation area and extent estimation under vegetation canopy from HR DEMs (Hashemi-Beni and Gebrehiwot, 2021).

A typical real-time HR urban floodwater mapping workflow can be organized in three procedures: (1) obtain HR DEMs, (2) extract visible floodwater extent from real-time HR optical images during flooding, and (3) estimate flood inundation depth and extent. Due to the high cost of LiDAR data acquisition and processing, HR DEMs are often available only in limited regions at a relatively recent time, making real-time HR flood mapping challenging to be applied extensively in practice. Inferring HR DEMs from existing low-resolution (LR) DEMs would be cost-effective and significantly benefit the purpose of urban floodwater mapping. Visible floodwater extraction from HR optical imagery can be processed as a pixel-wise image classification or a semantic segmentation task, but these procedures often require a significant number of training samples to train a model. Rapid data processing is required in disaster response, so a floodwater extraction method with little human interaction is desired. Moreover, flood mapping from incomplete water extent extracted from optical imagery due to shadows and vegetation is seldom addressed in the literature, so a hydraulic model needs to be assembled.

Therefore, this research paper aims to address existing challenges in HR urban flood mapping by proposing a novel rapid floodwater mapping framework, which can be divided into three components:

1. A new DEM upscaling method effectively reconstructs HR topographic details in urban regions from LR DEMs, so that areas without HR DEMs can better prepare for potential natural disasters, including floods.
2. A rapid visible floodwater extent extraction method from HR RGB remote sensing imagery takes a very limited amount of manual annotation, so that flood maps can be quickly produced in near real-time to benefit disaster response.
3. An accurate floodwater extent and depth estimation tool utilizing HR DEMs and visible floodwater extents, so that flood impact can be more accurately estimated to overcome the data acquisition limitations of HR optical imagery in shadows and vegetated regions.

This research conducts a case study with a real-world flood event to demonstrate the feasibility of applying the proposed multi-sensory urban flood mapping framework at a large urban scale for disaster response.

1.2. Related studies

1.2.1. DEM upscaling

The spatial resolution of DEMs determines the accuracy of flood mapping and modelling, and HR DEMs are especially desired in urban studies (Muhadi et al., 2020). However, HR DEMs are not always available in a given area, so enhancing the spatial resolution of DEMs could be a potential solution to this problem. Image super-resolution (SR) is a technology that generates HR images from LR images to meet the demand of resolution in various applications by using algorithms to surpass the limit of sensors (Fernandez-Beltran et al., 2017). Compared to conventional interpolation methods (e.g. bilinear, bicubic and lanczos), which tend to over-smooth the reconstructed HR images, learning-based algorithms that learn the relationship between multi-sensor and multi-resolution DEMs can improve the spatial resolution of DEMs, including a multi-scale Kalman smoother approach (Jhee et al., 2013) and an adapted multi-scale regularization method (Yue et al., 2015). As Xu et al. (2015) pointed out, DEMs are costly to obtain and are usually updated infrequently, so a single image SR method is more practical in DEM upscaling. With the recent advancement of deep learning methods, especially convolutional neural networks (CNNs), the single image SR task has made revolutionary progress in quantitative and qualitative evaluations (Wang et al., 2021). Early attempts have been made at DEM upscaling by directly applying an image SR network (i.e. SRCNN) to DEMs, and the results in the case study showed significant improvement over conventional methods (Chen et al., 2016). Demiray et al. (2021) applied the SRGAN image SR network to DEM upscaling, and the results indicated that the network performs well at flatter terrains but needs improvements in steeper areas. Compared to most research that trains the SR models with synthetic LR-HR DEM pairs, where corresponding LR DEMs were produced by downscaling and degrading HR DEMs, Wu et al. (2021) used real-world DEMs to train a network to simulate the WorldDEM at 12 m resolution from the shuttle radar topography mission (SRTM) DEM at 30 m resolution, and the experiments showed that the real-world training data produced better results. Zhang and Yu (2022) conducted a comparative study on applying three popular single-image SR networks (i.e. SRGAN, ESRGAN, CEDGAN) in the DEM upscaling task, and the results indicated that CNNs do not necessarily produce better results in the DEM upscaling task. Instead of directly adapting single-image SR networks, Xu et al. (2019) introduced edge detectors as an image gradient before training the proposed network, and the addition of gradient was demonstrated to be effective in two single-image SR networks (i.e. SRCNN and EDSR).

Despite some success in applying single image SR methods in DEM upscaling, these methods are based on an ill-posed assumption that high-level details can be reconstructed without extra information for reference (Yue et al., 2016). Image resolution can also be improved with spatial information taken from a different sensor at a higher spatial resolution with a fusion method, and one of the most well-known strategies in remote sensing is pan-sharpening. Pan-sharpening utilizes an HR panchromatic image to improve the spatial resolution of the multi-spectral images by taking advantage of the HR spatial features at a different spectral frequency (Meng et al., 2019). Since HR and VHR optical images are ubiquitously available at a much lower cost than LiDAR DEMs, they could provide HR spatial details of the terrain despite vegetation and objects covering the ground surface. Therefore, a fusion approach utilizing the HR optical imagery to improve the spatial resolution of LR DEMs would be a promising approach instead of directly upscaling the LR DEMs. Argudo et al. (2018) experimented with a fully convolutional network which utilizes deep feature hierarchies encoding to combine features at different scales to perform terrain SR using an aerial image fusion method to produce 2 m resolution DEMs from downsampled 15 m resolution LR DEMs. Kubade et al. (2021) further developed an attention feedback network using the same DEM dataset to take advantage of a recurrent structure to focus more on the

initial layers of the networks to enhance some key features of terrains. Compared to mountainous regions, where vegetation usually covers terrains, urban regions feature complex buildings and infrastructure. Amirkolaee and Arefi (2021) proposed a multi-scale deep network to produce an HR digital surface model (DSM) from SRTM DEMs utilizing corresponding HR satellite images, but this study was based on the task of urban height estimation from satellite images without learning terrain features from the LR DEMs. In summary, there are limited studies on urban DEM upscaling with a fusion approach using HR optical images and LR DEMs.

1.2.2. Flood mapping with remote sensing imagery

Remote sensing images, including both optical and SAR images, have been widely used in real-time flood mapping, especially in rural regions (Joyce et al., 2009). SAR images are very sensitive to open water regions with low backscatter values, which help identify flooded regions by comparing during and before flooding images (DeVries et al., 2020). More recently, deep learning models have demonstrated very effective in detecting surface water from medium-resolution SAR sensors such as Sentinel-1 when trained on well-labelled datasets such as Sen1Floods11 (Bonafilia et al., 2020). However, SAR images do not work well in urban regions, especially in dense built-up areas, due to complex urban structures, i.e. specular reflections from smooth asphalt and buildings, shadows and overlay effects of tall buildings (Mason et al., 2010). Tanguy et al. (2017) compared the floodwater classification accuracy with ultra-fine RADARSAT-2 images in both rural and urban regions, and the results in urban areas are more than 10% less accurate compared with rural areas using the same method. Low to medium-resolution optical images like MODIS and Landsat images provide floodwater mapping capability at a regional scale, and long-term monitoring and retrospective research capabilities of flood mapping over a large region (Mueller et al., 2016). However, the medium resolution optical images cannot provide enough details characterizing urban features, which provides limited benefits in urban areas.

Arithmetic indices calculated from combinations of different spectral bands of the optical sensors are commonly used for water mapping, such as the normalized difference water index (NDWI), the modified NDWI (MNDWI), the water ratio index (WRI), and the automated water extraction index (AWEI). The NDWI was proposed by McFeeters (1996) for the Landsat satellites by calculating the ratio between the near infra-red (NIR) and the green band, inspired by the well-known normalized difference vegetation index (NDVI). Afterwards, the short-wave infrared (SWIR) was found to be more reliable in built-up areas, and the MNDWI was proposed by taking the SWIR band in Landsat (Xu, 2006). The WRI was used by Shen and Li (2010) to extract water bodies from Landsat ETM+ images by taking the red band into consideration. To improve water and nonwater separability in dark built-up areas and shadow-infested areas, AWEI was proposed with two indices to automatically extract water areas from Landsat images to accommodate the two circumstances (Feyisa et al., 2014).

For real-time flood mapping during disaster response, airplanes and UAVs are often considered more desirable than optical satellite images due to the flexibility of data collection, the higher spatial resolution, and the operability under cloud layers in bad weather (Zhang and Crawford, 2020). However, unlike typical optical satellite sensors, imaging sensors mounted on airplanes or UAVs are usually digital cameras without the capability of capturing infrared bands. As a result, the aforementioned water indices that rely on infrared bands may not directly apply in floodwater extraction from aerial photos and UAV images. Several methods have attempted to use only RGB bands in floodwater extraction. Gerl et al. (2014) adopted a decision-tree classifier to perform land cover classification using pan-sharpened IKONOS RGB images. Feng et al. (2015) utilized grey-level co-occurrence matrix (GLCM) features in addition to the RGB spectral features to identify flooded areas using a random forest classifier from UAV images during a flood event. Zhang et al. (2019) proposed a flood water index (FWI) for turbid floodwater detection using RGB bands to work with both satellite and aerial images. More recently, deep learning methods, especially CNNs, have shown advantages in processing HR and VHR optical images due to the powerful spatial feature learning capability compared with conventional pixel-wise and object-wise classification techniques in urban flood mapping by treating it as a semantic segmentation problem (Gebrehiwot et al., 2019). However, due to the scarcity of training samples for HR flood images, data augmentation and other techniques are necessary to avoid overfitting in training deep learning networks for floodwater extraction (Hashemi-Beni and Gebrehiwot, 2021). With more and more openly accessible HR optical satellite and UAV images, datasets for developing deep learning models for flood monitoring have emerged recently, such as FloodNet (Rahnemoonfar et al., 2021) and SpaceNet 8 (Hänsch et al., 2022), making transfer learning a viable solution to overcome the limitation of training samples.

1.2.3. Flood mapping with DEM

Real-time mapping from optical images during flood events can extract visible floodwater extent, but the complete flood extent and flood depth estimation typically require a DEM as the input of flood models (National Research Council, 2007). The resolution and accuracy of DEMs are vital in flood modelling, and HR DEM is especially important in dense urban regions where small features like road curbs would affect the determination of inundation areas. LR DEMs allow a rapid flood simulation but will result in a large loss of information, including inundation extent, flow depth and flow velocity (Haile and Rientjes, 2005). HR DEM generated from airborne LiDAR has been demonstrated to have the highest accuracy in inundation estimation than other DEM sources including digital photogrammetry and interferometric synthetic aperture radar (IfSAR) (Casas et al., 2006). A finer resolution DEM is required for fine local-scale inundation predictions for flood management decisions in dense urban regions (de Almeida et al., 2018).

Typical physical hydraulic models take DEM as the primary input and solve 1D or 2D shallow-water equations (Warren and Bach, 1992). 2D models are the most widely used models in flood mapping and flood risk analysis, and some commonly used 2D models include ANUGA, FloodFlow, MIKE FLOOD, TUFLOW, HEC-RAS (Teng et al., 2017). Compared with the complicated hydrodynamic models, which require a huge amount of calculations, simplified flood models rely little on physical process simulation and directly predict the final flood state (Néelz and Pender, 2010). These methods are often faster to calculate in applications that do not require accurate flow dynamics, and some representative simplified models include the Rapid Flood Spreading Method (RFSM) and the Height Above the Nearest Drainage (HAND) model (Teng et al., 2017). The physical hydraulic models predict water movement from a pour point, but complex urban infrastructures, especially sewer systems and underground structures, make them difficult to accurately predict flood impact with sufficient supporting infrastructure data, as sewage overflow may occur in addition to overland flow in urban environments (Maksimović et al., 2009). Moreover, the computational complexity and input requirements make physical models undesirable in urban environments at a very high resolution, especially for real-time or near real-time flood mapping during disaster response (de Almeida et al., 2018). As a result, simplified inundation models with GIS software would be more practical and efficient in time-critical flood mapping scenarios (Cohen et al., 2018).

For coastal flood mapping, the flood extent and depth can be directly estimated by setting a flood elevation according to historical water gauge readings (Webster et al., 2006), but this kind of method has significant limitations in mapping river floods as a large area may contain several watersheds and flood elevation may change along the river (Zhang and Crawford, 2020). For pluvial and fluvial floods, the flood extent is usually extracted from remote sensing images, and the flood depth is then estimated by subtracting the DEM from the inferred floodwater elevation. To account for changes in water elevation, Huang et al. (2014) split flooded areas into small tiles to fill DEMs to inferred

water elevations assuming the flood surface is flat at a local scale. This idea was further developed to estimate the flood elevation of each extracted floodwater polygon to calculate flood depth by extracting statistical elevation values at boundary cells, such as mean (Gebrehiwot and Hashemi-Beni, 2021) and percentile threshold (Cian et al., 2018). One of the widely applied GIS floodwater mapping tools, the Floodwater Depth Estimation Tool (FwDET), estimates boundary flood depth by firstly adopted focal statistics in the initial version (Cohen et al., 2018) and then utilized the Cost Allocation tool in ArcGIS to better accommodate coastal floods (Cohen et al., 2019). The FwDET further applied two filtering procedures to smooth the input DEM to mitigate the impact of outliers on boundary flood elevation estimation in the latest version (Peter et al., 2022).

However, these methods only account for areas under visible flood extent, and floodwater mapping under vegetation canopy and in shadows is still challenging as visible floodwater boundaries do not necessarily correspond to 0 floodwater depth. Hashemi-Beni and Gebrehiwot (2021) attempted to infer flood extent under vegetation by applying region growing from remote sensing image derived visible floodwater extent, but the seed points were still manually selected with regard to the land cover type and water gauge readings. More recently, Bryant et al. (2022) proposed an inundation estimation tool called RICorDE which utilizes HAND values to correct potential errors in estimated flood polygons, but this tool has not been publicly released yet. Therefore, an automated rapid flood depth and extent estimation tool that utilizes incomplete visible flood extents with shadows and vegetation canopy is still in demand.

2. Methods

2.1. Study area

The study area of the proposed research is located in the city of Calgary, Alberta, Canada, the third most populous city in Canada. The Bow River flows through Calgary, and the Elbow River intersects the Bow River in the downtown region. In June of 2013, an unprecedented flood event occurred in Alberta due to excessive precipitation, resulting in the most significant flood event on the Bow River since 1932. As a result, Calgary experienced extensive flooding in the urban region, which caused the evacuation of approximately 100,000 people. The estimated damage caused by this flood was over $5 billion (City of Calgary, 2021). The specific study area is the flooded zones within downtown Calgary, covering approximately 4.9 km by 6.5 km, as shown in Fig. 1. The study area comprises various urban landscapes, including dense high-rise buildings, low-rise residential, low-rise commercial buildings and urban vegetation. Though timely HR aerial imagery was collected just after the peak of the flood event, the complex urban structure, shadows, and vegetation coverage made it difficult to delineate the complete flood extent and depth directly from the RGB imagery. Therefore the proposed method aims to estimate urban flood extent with multi-sensory data efficiently and accurately.

2.2. Overview of the proposed framework

A flowchart of the proposed study is shown in Fig. 2. The proposed research intends to produce accurate near real-time flood mapping combining aerial imagery during the flood and a pre-event HR DEM upscaled from existing data utilizing deep neural networks. The proposed multi-sensory flood mapping framework consists of three components. (1) DEM upscaling from an LR existing DEM and an HR aerial imagery before the flood event to produce an HR DEM with a deep neural network. (2) Visible floodwater extraction from RGB aerial imagery acquired during the flood with a semantic segmentation deep neural network. (3) Using the extracted visible floodwater extent as a guide to estimate flood inundation extent with a GIS-based tool. The detailed methods proposed for this study are discussed in the following sections.

This research intends to validate the proposed flood mapping framework in a real-world flood scenario, the 2013 Calgary flood. The highest quality publicly accessible DEM in Calgary before 2013 was the Canadian Digital Elevation Model (CDEM) with an approximate resolution of 18 m, which is not effective in producing HR flood mapping. An aerial image of Calgary with 25 cm resolution was taken in 2012, which was before the flood event, is used in the DEM upscaling process to reconstruct HR urban elevation details. The proposed DEM upscaling method upscales the CDEM 9 times into a 2 m resolution HR DEM with the support of the aerial imagery. Next, aerial imagery taken by the City of Calgary on June 22nd, 2013, after the peak of the flood event, covering the major urban areas along the Bow River in Calgary at 20 cm resolution was used to extract visible floodwater extent. A detailed floodwater extent polygon dataset provided by Natural Resources Canada through manual digitization was used as the ground truth for validation. Finally, the proposed GIS-based flood mapping tool produces an estimated flood extent and flood depth map with the upscaled HR DEM and the visible floodwater mask. The data used in this research are summarized in Table 1.

To evaluate the performance of the proposed flood mapping framework, several metrics were adopted to quantify both the completeness and correctness of the floodwater extent prediction, including overall accuracy (OA), precision (or user's accuracy), recall (or producer's accuracy), $F1{-}score$ and intersection-over-union (IoU). In a confusion matrix, an observation of predictions are compared with the ground truth to be categorized into true positive (TP), true negative (TN), false positive (FP) and false negative (FN). The evaluations are defined as follows:

$$Accuracy = \frac{\sum(TP + TN)}{\sum(TP + FP + FN + TN)} \tag{1}$$

$$Precision = \frac{\sum TP}{\sum(TP + FP)} \tag{2}$$

$$Recall = \frac{\sum TP}{\sum(TP + FN)} \tag{3}$$

$$IoU = \frac{\sum TP}{\sum(TP + FP + FN)} \tag{4}$$

$$F1{-}score = \frac{2 \times Precision \times Recall}{Precision + Recall} \tag{5}$$

2.3. DEM upscaling network with aerial imagery fusion

An image fusion network is proposed to reconstruct an HR DEM from an LR DEM with support from an HR optical image in urban regions. Different from conventional image fusion tasks such as pan-sharpening, the optical images do not directly present correspondence with the underlying topography, but some latent relation with urban features such as building and tree height in less dense vegetated areas could be explored with deep learning models (Mou and Zhu, 2018). The proposed DEM upscaling network focuses on the potential added topographic details in HR DEMs in urban regions, such as roads, buildings, and infrastructure, which cannot be well-represented in LR DEMs but may serve as the passage or obstruction for urban floods. These urban features are usually built according to similar building codes or standards, so in this research, the HR topographic details are assumed to be comparable across different regions and urban terrains regardless of the LR topography underneath. An LR DEM base map in an urban area could be viewed as a coarse representation of the terrain without details, changes made on the terrain surface, such as construction of roads and buildings, can be reflected on the HR optical imagery. Therefore, the proposed method aims to infer the elevation difference between corresponding HR and LR DEMs directly from HR optical imagery. Adding the detailed elevation differences to the LR DEM, an HR DEM with topographic details could be reconstructed to improve the potential flood mapping capability of the LR DEM when a higher quality DEM is not available.

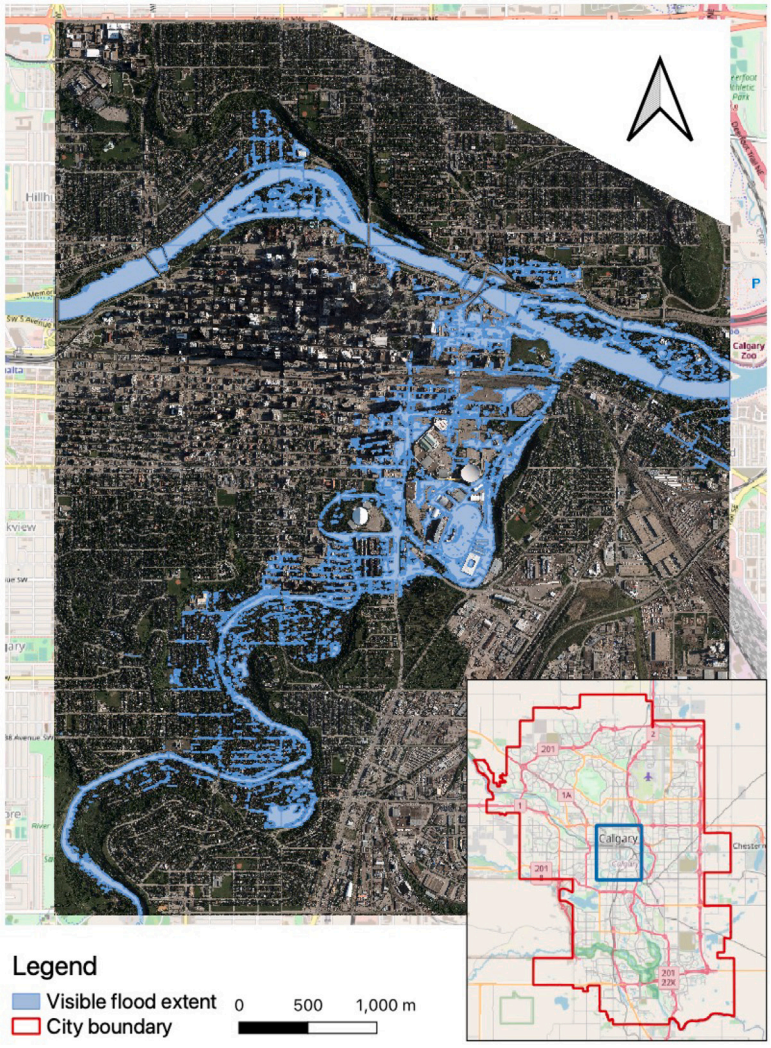

Fig. 1. The study area in Calgary, Canada.

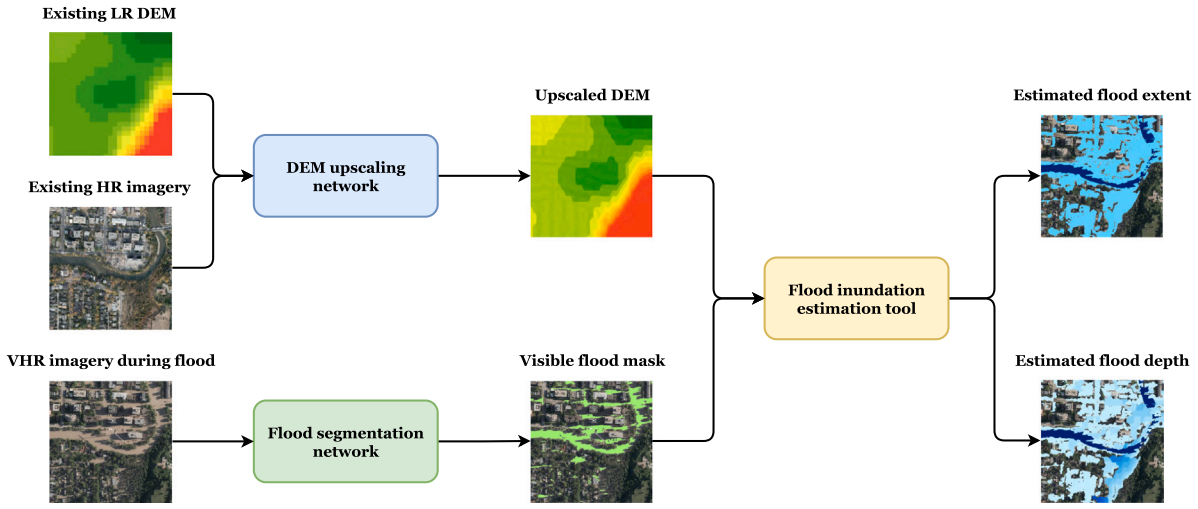

Fig. 2. Overview of the proposed flood mapping framework.

Inspired by the depth completion CNN model proposed by Ma et al. (2019), DEM resolution enhancement is formulated as a deep regression problem from two inputs, an LR DEM and a corresponding HR RGB image in this work. The proposed network adopts a 5-layer encoder-decoder architecture, where the ResNet-34 (He et al., 2016) is adopted as the encoder and transposed convolution blocks with 3 × 3

Table 1
List of data.

Dataset	Source	Resolution	Usage
Ontario LiDAR DEM	Government of Ontario	2 m	Train DEM upscaling network
Ontario Orthoimagery	Government of Ontario	20 cm	Train DEM upscaling network
Canadian CDEM	Government of Canada	18 m	Produce upscaled DEM in Calgary
2012 Calgary Orthoimagery	City of Calgary	25 cm	Produce upscaled DEM in Calgary
FloodNet image dataset	Rahnemoonfar et al. (2021)	1.5 cm	Train floodwater extraction network
2013 Calgary Orthoimagery	City of Calgary	10 cm	Train floodwater extraction network and produce floodwater extent
Calgary floodwater polygon	Natural Resources Canada	–	Train floodwater extraction network and validate produced flood maps
Calgary floodwater extent	City of Calgary	–	Validate produced flood maps
2012 Calgary LiDAR DEM	City of Calgary	20 cm	Validate produced flood maps

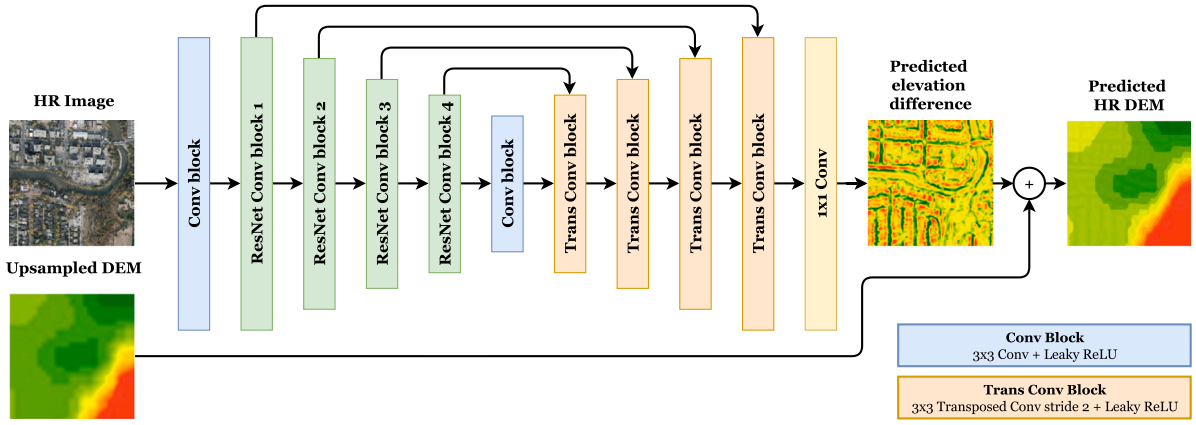

Fig. 3. Overview of proposed DEM upscaling network.

convolutions with stride 2, followed by a 1×1 convolution layer to produce the inferred HR topographic details. The output from each encoding layer is concatenated with the input of the corresponding decoding layer using skip connections with a similar strategy as UNet (Ronneberger et al., 2015). Finally, the predicted elevation differences are added to the interpolated DEM to produce the inferred HR DEM. The proposed DEM upscaling network structure is summarized in Fig. 3.

HR DEMs and corresponding HR RGB images are required to train this model. The 2013 South Central Ontario Orthophotography (SCOOP) (OMNRF, 2013), the 2014 Digital Raster Acquisition Project Eastern Ontario (DRAPE) (OMNRF, 2014), and the 2015 Southwestern Ontario Orthophotography Project (SWOOP) (OMNRF, 2015), which include georeferenced orthoimages at 20 cm resolution and LiDAR-derived DEM at 2 m resolution pairs, were selected. The major urban areas within the three datasets, such as Kitchener–Waterloo–Cambridge, Ottawa–Gatineau, Hamilton, Kingston, etc., were chosen as the training area due to the similarity of urban structures to the city of Calgary. The proposed network first upsamples an 18 m-resolution CDEM to 2 m with bicubic interpolation to match the output DEM resolution of 2 m. To simulate this process, the HR DEMs were downscaled to 18 m to approximate the actual LR CDEM, and then were interpolated to a 2 m resolution as the network input. The RGB orthoimages and HR DEMs were also downscaled to 2 m to match the input and ground truth resolution. The elevation difference between the 2 m DEM ground truth and the interpolated LR DEM was used as the inference target. Considering the significant absolute and relative elevation differences in different areas, previous research on DEM upscaling either used log transformation (Wu et al., 2021) or tile-wise normalization (Zhang and Yu, 2022) to standardize the elevation values, but these methods may not represent the elevation distributions well if applied in a different region at a different spatial resolution or a different tile size. Based on the assumption that the elevation differences between the LR and HR DEMs in urban areas are consistent regardless of the topography, normalization of elevation values is not needed in this model design.

To train this network, the L2 loss (mean squared error (MSE)) was used as the loss function to preserve sharper changes in urban elevation around buildings and infrastructure, instead of the common L1 loss (mean absolute error (MAE)) which may overly smooth the reconstructed results (Wang et al., 2021). The image augmentations include random flipping, rotation and centre cropping to 384×384 pixels. The ADAM optimizer (Kingma and Ba, 2015) with a learning rate of 1×10^{-4} was adopted. Aerial imagery of Calgary taken in September 2012 before the flood was used as the HR RGB image input to guide the network. Finally, with the CDEM and the RGB aerial imagery, an HR DEM of the area of interest was produced to predict an HR DEM to support HR flood mapping. The DEM upscaling network was implemented using PyTorch (Paszke et al., 2019).

2.4. Floodwater extraction network with transfer learning

Timely response during flood events requires the least amount of manual labelling, so it is not feasible to produce a large number of training samples for deep neural networks in real-world disaster response scenarios. In addition, timely optical images are rarely collected during flood events due to the limitation of weather and resources, which further limits the available number of training samples. As a result, transfer learning, which takes advantage of features learned by deep neural networks on other datasets, is a sensible choice for visible flood mapping to reduce manual annotation. Studies using CNN models to extract floodwater from HR RGB images have attempted transfer learning (Gebrehiwot et al., 2019; Hashemi-Beni and Gebrehiwot, 2021), but transferring weights trained on a universal image dataset such as ImageNet (Deng et al., 2009) may not be the most suitable method for the flood mapping task from remote sensing images. As more public datasets have been released, taking advantage of flood datasets would be more effective for transfer learning in this study. The FloodNet dataset (Rahnemoonfar et al., 2021), which is a UAV image dataset collected during Hurricane Harvey in Texas in 2017, contains approximately 400 labelled VHR RGB images at the resolution of 1.5 cm would provide substantial guidance for the flood extraction network due to the scarcity of accessible images during flood events.

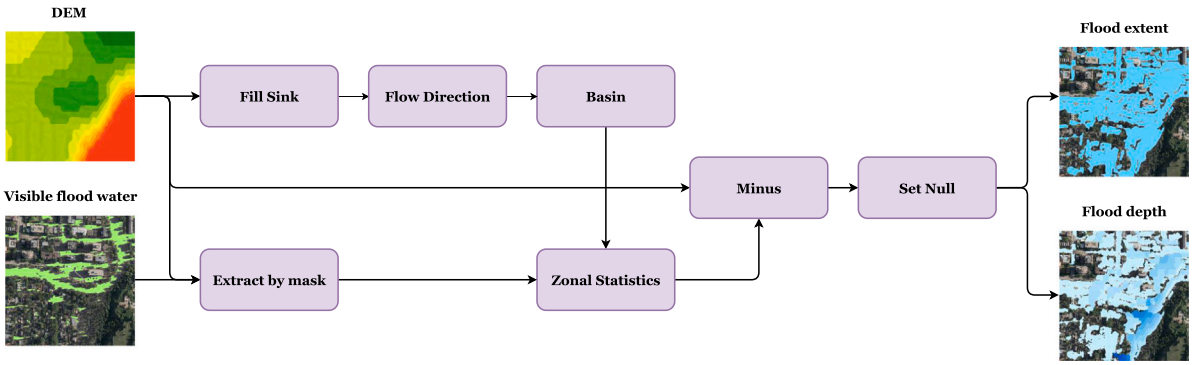

Fig. 4. Workflow for proposed floodwater mapping tool.

A CNN network based on DeepLabV3+ (Chen et al., 2018) was utilized to accurately map the visible floodwater extent from the real-time RGB aerial imagery of Calgary in 2013. In this study, the ResNet-50 (He et al., 2016) network was adopted as the backbone. The atrous convolution layer was applied in the encoder and decoder. Depth-wise separable convolution was also applied in the atrous spatial pyramid pooling (ASPP) in the encoder. A two-stage fine-tuning process was adopted for transfer learning due to the lack of labelled images during flood events. The labelled images of the FloodNet dataset were down-sampled 10 times to reach a similar resolution to that of the Calgary aerial imagery. The limited samples make the classifier prone to overfit, so the first fine-tuning process was based on the weights pre-trained on the ADE20K dataset (Zhou et al., 2019). Since FloodNet is a multi-class semantic segmentation dataset, the cross entropy loss was adopted as the loss function, and the ADAM optimizer with a learning rate of 1×10^{-5} was used.

The RGB aerial imagery of Calgary during the flood event was tiled into 1000 × 1000 pixel patches with the matching visible floodwater extent masks to reduce the computational cost of each image. Note that in this research, all permanent water bodies including rivers and ponds are treated as floodwater in the ground truth floodwater extent masks. In the second stage of transfer learning, a small percentage of the data was used for fine-tuning a binary segmentation network with the goal of requiring the least number of labelled images and the least amount of time possible. Since the flooded area only covers a small percentage of the imaged area, non-flooded image tiles were also sampled in addition to the flooded tiles in the training set to reproduce a similar distribution of the actual image to reduce the probability of overfitting. A weighted binary cross entropy loss was adopted to accelerate convergence, and the ADAM optimizer with a learning rate of 1×10^{-6} was used. Random flipping, rotation and centre cropping were adopted as image augmentation in both fine-tuning processes. The experiments were conducted using the MMSegmentation toolbox (MMSegmentation Contributors, 2020) and PyTorch.

2.5. Floodwater mapping tool with visible floodwater map and HR DEM

Due to the complexity of urban environments and drainage systems, it is challenging to estimate flood inundation areas using HR DEMs by setting a flood elevation. For flood risk predictions, some flood models could take drainage capacity into consideration to some extent, but these methods are not always achievable without a massive amount of supporting data about urban infrastructures (Mignot et al., 2019). However, it is feasible to predict inundation at a local level with guidance using visible floodwater information extracted from real-time aerial images since flood elevation can be assumed to be consistent in a local region (Huang et al., 2014). Some established methods, such as the FwDET (Cohen et al., 2018), assume boundaries of visible floodwater extent to have a water depth of 0, but this assumption is not the case when shadows and vegetation canopy are present. This research intends to account for potentially flooded areas in shadows and under vegetation canopy, which could not be directly extracted and are often underestimated from optical imagery. The HR DEM may not be sufficient to delineate complete urban drainage basins due to the complexity of urban stormwater infrastructure, but the local drainage basins derived using the proposed flood mapping tool can help complete the extent of the observed standing water from HR optical images to better assess the flood extent.

Before the full floodwater extent and depth mapping procedure, visible flood extent polygons extracted from HR imagery with an area under 16 m^2, which is equivalent to four pixels in the reconstructed 2 m DEM, were removed to reduce prediction outliers. Fig. 4 presents an overview of the floodwater mapping procedure. The main idea of the floodwater mapping procedure is to identify potential flood elevation at the local basin level. The floodwater depth estimation tool was implemented with ArcGIS Pro (ESRI Inc, 2021) Model Builder. Firstly, local basins or potential flood impact zones could be extracted from the DEM using hydrological analysis with the following steps (Jamali et al., 2018): (1) compute flow direction of each cell in DEM, (2) identify sinks, (3) fill sinks and identify watersheds, (4) extract watershed boundaries. Different from conventional river hydrological analysis where all sinks are filled, a threshold of 20 cm was used in the filling process to capture detailed urban water catchments along roads or small terrain depressions where urban shallow water movements prevail (de Almeida et al., 2018). The GIS tools used in this step include *Fill*, *Flow Direction*, and *Basin*. Afterwards, potential floodwater elevation within each watershed could be identified by overlaying the visible floodwater extent and the DEM. To reduce the impact of possible elevation outliers in HR DEMs, especially in the upsampled DEM from the proposed deep neural network, the 95th percentile (Cian et al., 2018) of elevation values in each basin is taken as the inferred floodwater elevation. The tool *Zonal Statistics* is applied in this step. Finally, a floodwater extent map can be produced by setting the elevation thresholds within each basin, and the floodwater depth map can also be produced by subtraction. The tools used in this step include *Minus* and *Set Null*. To produce the final floodwater extent and depth map for disaster response, the existing water bodies including rivers and lakes, need to be removed.

3. Results and analysis

3.1. Results of DEM upscaling

The proposed DEM upscaling method intends to regress the latent relationship between HR urban topographic details and the features in aerial images, so that the detailed topographic information could be added to a ubiquitously available LR DEM. In this study, the trained network was tested on the study area to upscale the CDEM at 18 m resolution into a 2 m resolution DEM with the support of aerial imagery taken in September 2012 before the flood event in the main urban

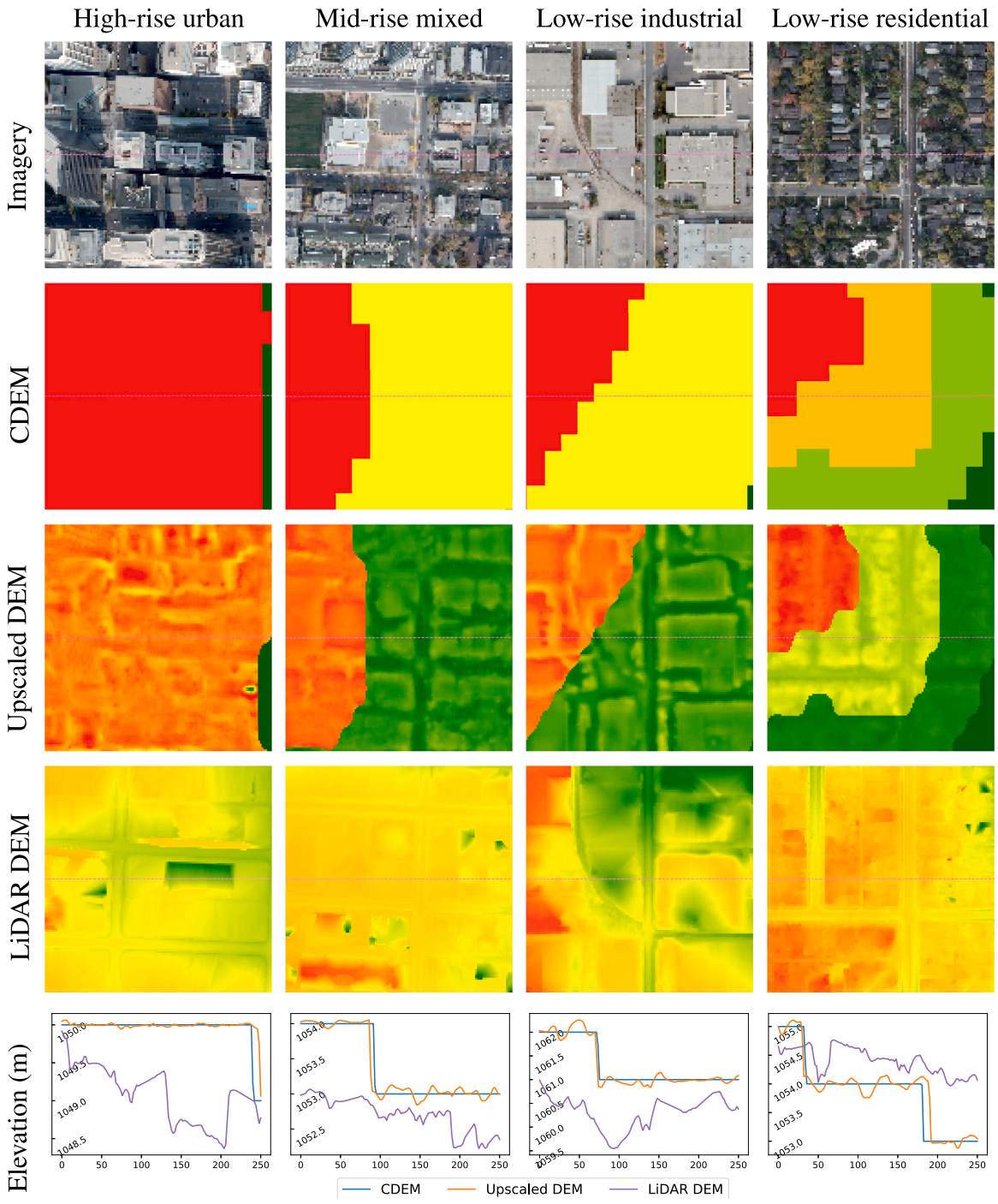

Fig. 5. Results of DEM upscaling using CDEM and an aerial imagery in Calgary 2012 in four typical urban land use types. Each tile covers 250 × 250 m. Symbol colours were assigned per the statistics of each tile (green → red: elevation low → high). The DEM profiles were extracted by the dashed line in the middle of the windows.

area of Calgary. An HR DEM with 0.5 m resolution produced by an airborne LiDAR sensor in 2012, before the flood event, was used as a comparison. Some examples of DEM upscaling results are shown in Fig. 5, where all the images and DEMs were resampled to 2 m resolution for a fair comparison.

In Fig. 5, samples of four typical urban land use types, including urban centres with high-density high-rise buildings, mixed areas with mid-rise residential and commercial buildings, industrial areas with low-rise buildings with very large footprints, and typical north American residential areas with low-rise buildings, were illustrated, together with a comparison of elevation profiles in the sample areas. Among these areas, the high-rise urban regions are often affected by building shadows, and the low-rise residential areas are often partially covered by vegetation canopies. From the DEM upsampling results, some urban features which could highly affect urban runoff, including roads and building footprints, were reconstructed with more details from the HR aerial imagery and added to the LR CDEM. In areas with low-rise buildings where the road features are clearly visible, the upscaled DEMs show stronger correspondence with the geometric features from the optical imagery, while in areas with high-rise buildings or heavier vegetation canopy, the reconstructed urban details may be less significant due to limited correlation between the optical features from the rooftops or tree canopies and the underlying topography changes. In light-vegetated urban areas such as the low-rise residential area shown

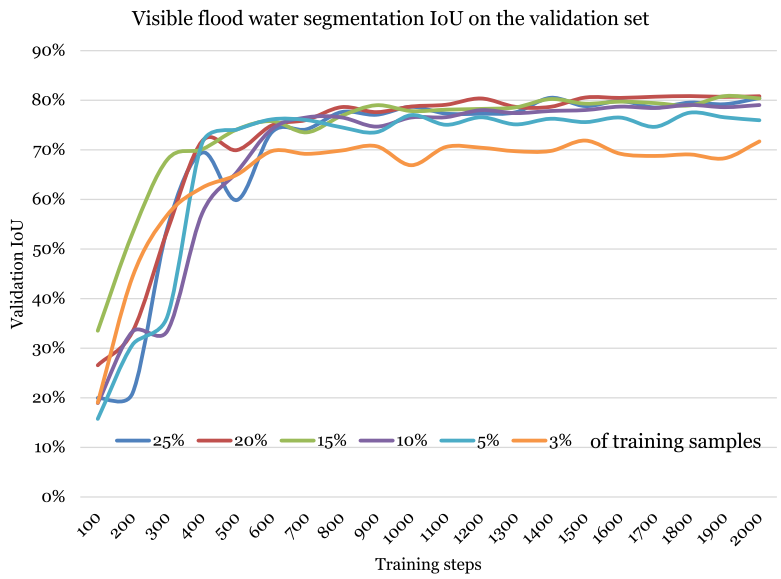

Fig. 6. Visible floodwater segmentation evaluation using a small proportion of the training set.

in Fig. 5, some buildings and roads are covered by sparse trees but the proposed DEM upscaling method can still reconstruct elevation details reasonably well by comparing the DEM samples and the profile. The convergence of the network and the improved DEM upscaling results have validated the assumption that those targeted urban elevation details could be reconstructed from HR optical images to some degree. Although significant differences still exist when compared with the LiDAR DEM, majorly due to the low accuracy and precision of the LR CDEM, which could not be magically improved without actual field measurements, the upscaled DEM with reconstructed HR topographic details would benefit flood mapping at a local scale.

Due to the significant acquisition time difference between the CDEM collected before 1990 in the study area and the LiDAR DEM, the topography may have changed to some degree in urban regions due to urban redevelopment. More importantly, the vertical precision of 1 m in the LR CDEM would result in absolute errors of over 1 m compared with the LiDAR DEM while the local elevation changes are at a much smaller scale, so a quantitative evaluation of the upscaled DEM in absolute elevation values is not meaningful to reflect the improvement of DEMs in this research. Instead, the improvements in DEM by upscaling will be indirectly compared in the application of urban flood mapping in Section 3.3. The differences between common types of DEM products in the study area are discussed further in Section 4.1.

3.2. Results of visible floodwater extraction

A transfer learning strategy with two-stage fine-tuning was proposed to effectively extract visible floodwater from real-time RGB aerial imagery with limited human labelling in disaster response scenarios. The intention is to use as few labelled samples as possible to produce an acceptable accuracy so that decision-makers can better estimate flood damages during flood events. 75% of both the aerial image tiles and the corresponding visible floodwater polygons were selected with a stratified random sampling of both flooded and non-flooded tiles to evaluate the performance of the network trained on different proportions of the training samples (25%, 20%, 15%, 10%, 5% and 3% of the total image tiles). The $IoUs$ of the experimental results are shown in Fig. 6. It can be observed that using a larger proportion of tiles would produce a higher floodwater prediction accuracy and a faster convergence at the same time. The performance of the network significantly decreases when the portion of training tiles is less than 10% of the total amount. Given the similar amount of training steps, which is approximately equivalent to the training time, needed for each testing case, the fewer number of training samples needed, the less time would be spent on manual interpretation of the near-real-time aerial imagery. By comparing the results of the experiment, using 10% of the labelled tiles for transfer learning would be reasonable to balance the short manual labelling time and the high floodwater extraction accuracy. In this study, approximately 1500–2000 training steps were needed for the network to achieve steady performance, and it takes approximately 10 min on a machine with one NVIDIA RTX 2080 Ti GPU with 11G graphic RAM. Therefore, the visible floodwater prediction results obtained from the network trained on 10% of the tiles were adopted as the input of the later floodwater mapping model to reflect a possible operational environment. In this case, an IoU of 80.0% and a producer's accuracy of 85.2% on the visible floodwater were achieved. Meanwhile, the OA of the floodwater-background classification achieved 98.6%.

Compared with previous methods where only selected local regions were tested (Zhang and Crawford, 2020; Hashemi-Beni and Gebrehiwot, 2021), the proposed method has extracted the visible floodwater from the aerial imagery with very high accuracy in the whole study area in a large scale, especially in regions not affected by the flood. A detailed visual evaluation of the visible floodwater extraction result derived from the proposed method is shown in Fig. 7 and four representative areas are zoomed in on the right. The areas shown in blue represent the correct prediction of visible floodwater extent, and the visual distribution in Fig. 7 demonstrates the high validation IoU of over 80%. Minor floodwater prediction errors can also be observed with the yellow colour showing the missed predictions and the blue colour showing the false predictions. From Box 1 and Box 3, it can be observed that despite the complex shape of vegetation, the predicted visible floodwater area aligns well with the manual interpretation with some minor errors in mixed regions contaminated by shadows. From Box 2, due to the similarity of colour, shallow floodwater is difficult to be distinguished from concrete impervious surfaces. Moreover, the prediction of floodwater in bare earth areas of construction sites is difficult for this method as shown in Box 4, but the water surface in these areas may not be caused by river overflow in this study area.

3.3. Results of floodwater mapping

A GIS workflow combining several hydrological processes was proposed to predict flood inundation depth at the local basin level using

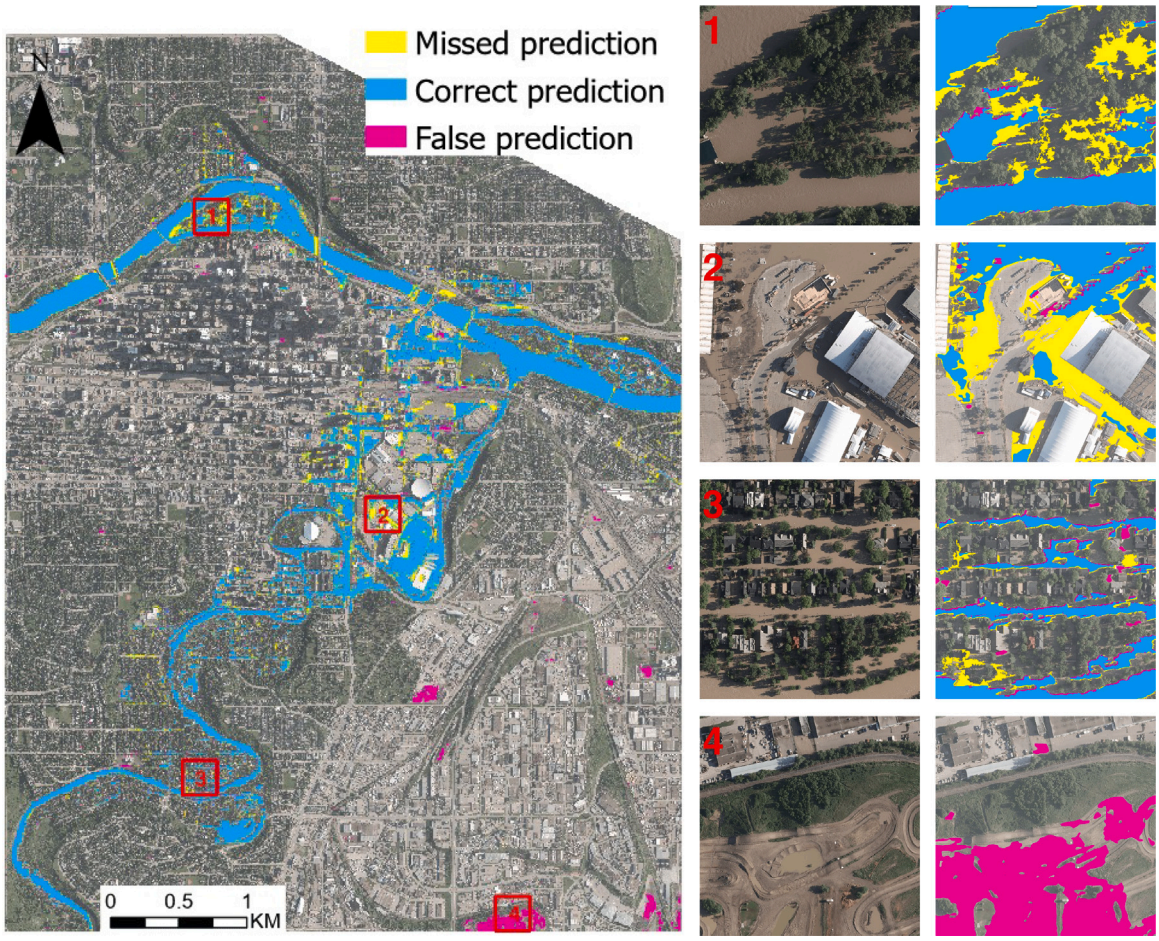

Fig. 7. Visual illustration of visible floodwater extraction errors from the imagery of the 2013 Calgary flood. Detailed comparisons of the aerial images and the predictions in each red box ordered from top to bottom are shown on the right. Each red box covers 250 × 250 m.

visible floodwater polygons and HR DEMs, and local floodwater extent could be estimated in areas in shadows and under vegetation canopy. Compared with existing flood depth estimation tools, the proposed GIS tool can simultaneously produce a floodwater extent map and a flood depth map. Fig. 8 compares the flood extent prediction results using both the CDEM at 18 m resolution (Fig. 8(a)) and the upscaled DEM at 2 m resolution (Fig. 8(b)) according to the predicted floodwater extent. A reference flood extent prediction using the manually labelled visible floodwater polygons and the HR LiDAR DEM in 2012 at 0.5 m resolution (Fig. 8(c)) is shown as a reference to the 2013 Calgary flood. Although the reference flood extent may have some limitations, it is the best estimate without a detailed hydraulic model by visually comparing the floodwater extent and the HR optical imagery during the flood event. In addition, a flood extent polygon produced by the City of Calgary is also presented in Fig. 8(d) for a visual comparison. For a quantitative evaluation of the proposed flood mapping workflow, the flood extents produced from various floodwater extent sources and different combinations of flood extent and DEMs are compared in Table 2. In this table, the floodwater polygons are compared with the reference flood extent and evaluated in Precision (Eq. (2)), Recall (Eq. (3)), IoU (Eq. (4)), and $F1{-}Score$ (Eq. (5)). In addition, the flood area differences were also compared both in terms of area and percentages.

Some detailed comparisons between the predicted flood extent with the proposed workflow (Fig. 8(b)) and the reference flood extent (Fig. 8(c)) are shown in the lower right corner in Fig. 8. It can be observed that building shadows and vegetation canopy are prevalent in urban areas, which resulted in the significant underestimation of the flood extent by using optical images only, so an HR DEM input into the proposed flood mapping tool is indispensable to delineate flooded areas accurately. The predicted flood extent from the proposed framework using the upscaled DEM and the image-extracted visible floodwater extent is very similar in visual comparison with the reference flood extent, and this demonstrated that the upscaled DEM could reconstruct some topographic details that highly resemble the LiDAR DEM. In Box B, the shadows of the high-rise buildings limits the identification of floodwater extent from optical images, but with the detailed reconstruction of building footprints and roads, a more accurate flood extent can be estimated. In Box C and D, many cases can be found where the roads are flooded while the houses above the curbs are unaffected, which proves that roads may act as channels for floodwater flow and road curbs may play an essential role in dividing local flood basins. The improved flood extent estimation can be attributed to the successful reconstruction of topography details of urban roads during the DEM upscaling process. In Box D and the upper half of Box B, it can be observed that the performance of DEM upscaling is not compromised with sparse urban vegetation, but the improvement under more dense vegetation is less significant as shown in the lower half of Box B. However, some overestimation of floodwater extent prediction using the upscaled DEM is also observed in the four boxes, but they are much less significant compared with the results from the LR CDEM. Moreover, some flood extent prediction errors can also be observed in areas north of Box A, west of Box C and D, and some other areas away from the rivers, by comparing Figs. 8(b) and 8(c). These errors are mostly due to the visible floodwater extraction errors illustrated in Fig. 7.

After analysing the floodwater extent prediction results both qualitatively and quantitatively, some observations worth noting were made. First of all, it was found that extracting urban floodwater extent from

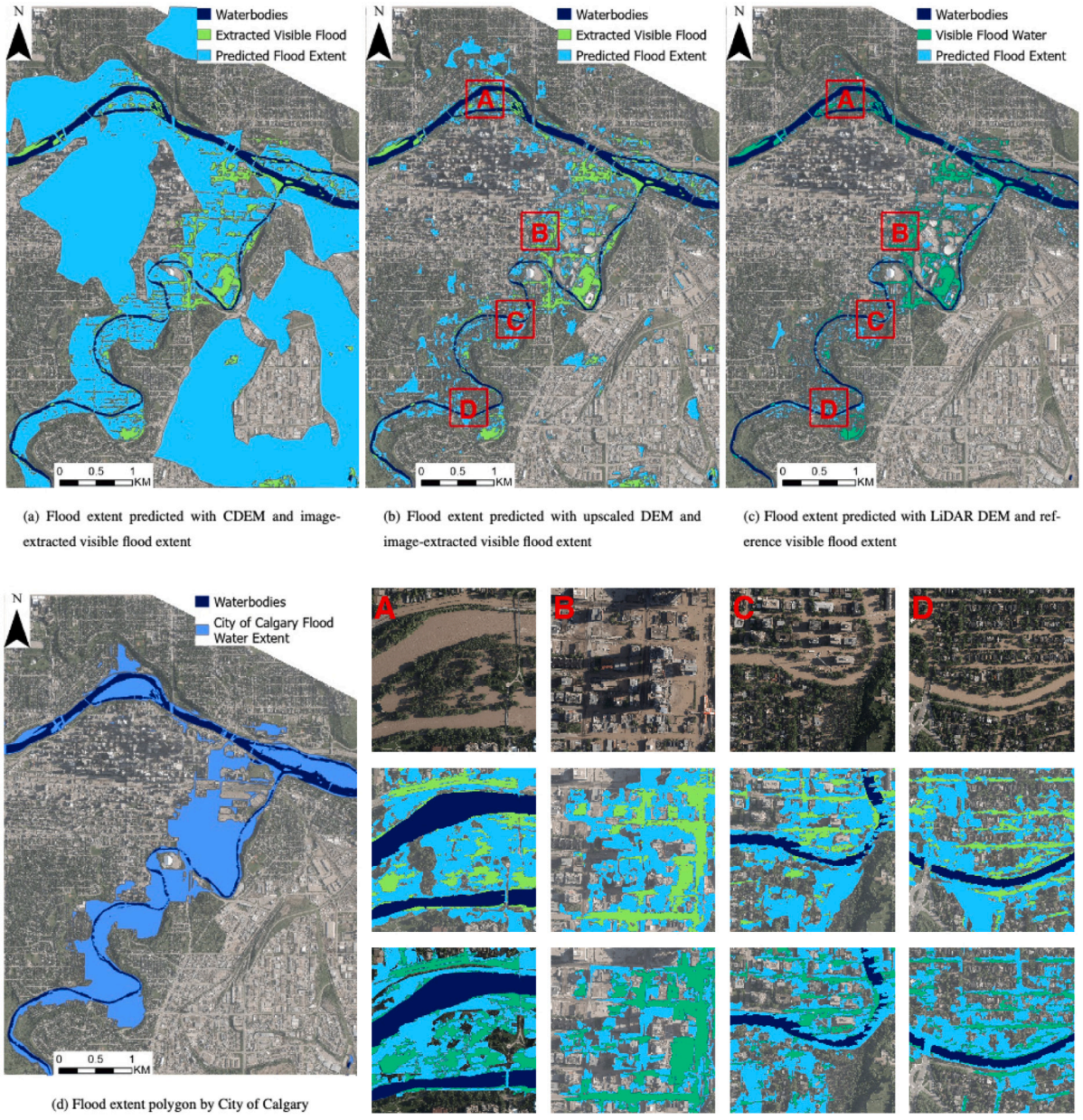

Fig. 8. Comparison of floodwater extents from different sources and predicted by different combinations of DEMs and visible floodwater extent polygons. Zoomed-in comparisons of the predicted floodwater extent in each red box A-D are shown in the lower right in the four columns, where the three rows from top to bottom represent the RGB aerial imagery, flood extent predicted from the upscaled DEM and the image-extracted visible floodwater extent (b), flood extent predicted with LiDAR DEM and the reference visible extent (c). Each red box covers 500 × 500 m.

Table 2
Quantitative evaluation of floodwater extent from different sources and predicted by different combinations of DEMs and visible floodwater extent polygons compared with the reference floodwater extent.

Floodwater extent	Precision	Recall	IoU	F1-Score	Area error (m^2)	Area error
Image-extracted visible flood extent	93.86%	38.58%	37.63%	54.68%	−2,743,261	−58.90%
Reference visible flood extent	97.80%	43.38%	42.96%	60.61%	−2,614,459	−55.65%
City of Calgary flood extent	72.28%	85.88%	64.60%	78.49%	+724,288	+18.81%
CDEM + extracted flood extent	21.88%	88.19%	21.26%	35.06%	+11,860,471	+303.02%
CDEM + ref. flood extent	45.65%	88.96%	43.20%	60.34%	+3,714,234	+94.89%
Upscaled DEM + extracted flood extent	59.33%	76.92%	50.37%	66.99%	+1,141,152	+29.64%
Upscaled DEM + ref. flood extent	69.62%	83.03%	60.95%	75.74%	+742,108	+19.27%
LiDAR DEM + extracted flood extent	61.21%	79.95%	53.06%	69.33%	+1,425,879	+30.61%

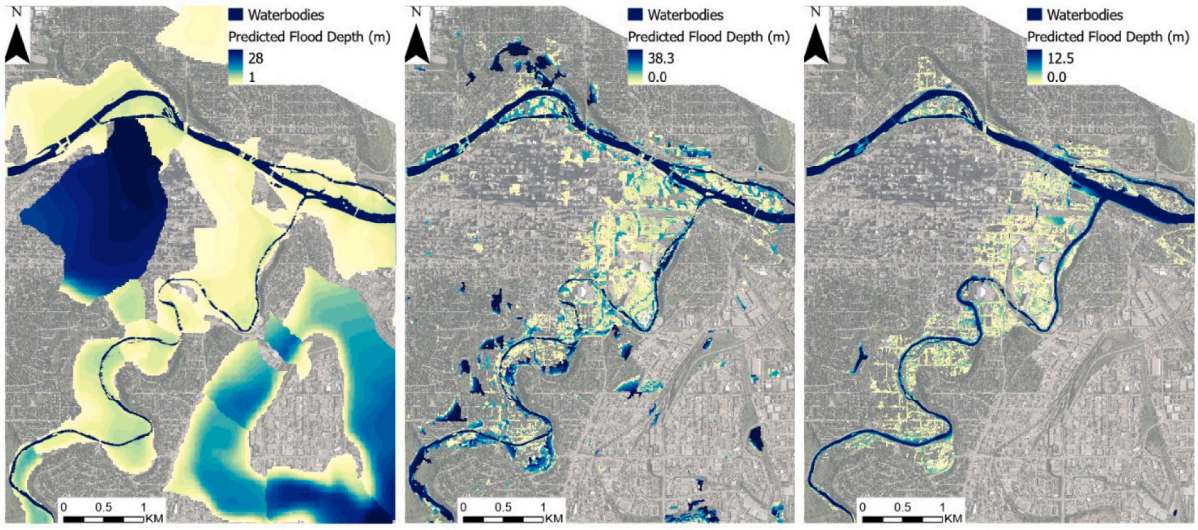

(a) Flood depth predicted with CDEM and image-extracted visible flood extent

(b) Flood depth predicted with upscaled DEM and image-extracted visible flood extent

(c) Flood depth predicted with LiDAR DEM and reference visible flood extent

Fig. 9. Floodwater depth prediction results.

optical images could lead to a significant underestimation of over 50% of the actual flood extent due to various factors such as occlusion from building shadows and tree canopies. Therefore, a high-quality HR DEM in urban regions is indispensable for producing HR floodwater maps. The flood extent and flood depth mapping methods that do not infer inundated areas under occlusions in optical images may also significantly underestimate flood damage in urban areas. Second, it can be observed that the use of LR CDEM resulted in a significant overestimation of the flood extent as shown in Fig. 8(a), especially in the high-density downtown area in the west and in the eastern part of the city away from the river. An LR DEM does not meet the requirement to produce accurate flood maps in urban regions due to the lack of urban topographic details and the limited elevation accuracy, and the LR DEMs are more prone to errors in visible floodwater extraction. Third, by comparing Figs. 8(d) and 8(c), it can be observed that the manually produced flood map by experts also overestimated the flood impact by over 18%. This flood map from the city may focus more on the total affected boundary rather than a detailed inundation map, so a flood map with a higher level of detail is still preferable in more detailed flood damage assessment. Finally, the predicted flood extent in Fig. 8(b) using the proposed flood mapping framework is significantly more accurate than that of LR CDEM in both qualitative and quantitative evaluation. The accuracy of floodwater extent mapping is reliant on the precision of both visible floodwater extraction and DEM. By comparing the flood extent prediction with different combinations of the two factors in Table 2, if the errors in the visible floodwater extraction could be reduced, the proposed flood mapping framework could produce a flood extent that is nearly as precise as the manually created flood map by the City of Calgary. Furthermore, when comparing the flood extent results using predicted visible floodwater extent, consistent performance can be observed in Table 2, regardless of whether an upscaled DEM or LiDAR DEM is used. As a result, the experiments indirectly proved that the urban topographic features reconstructed in the upscaled DEM could effectively delineate urban drainage basins, and could bring significant improvement over predictions with LR CDEM.

In addition to the floodwater extent, the proposed flood mapping tool also produces flood inundation depth estimation maps. A comparison of floodwater depth prediction results is illustrated in Fig. 9. From the comparison, the CDEM produced unsatisfactory results (Fig. 9(a)) in depth estimation with significant errors, especially in the downtown areas, compared with the predicted results using the upscaled DEM (Fig. 9(b)) despite using the same extracted floodwater extent. Fig. 9(b) has a few much deeper flood depth predictions compared with the reference flood depth map produced with the manually labelled floodwater extent and the LiDAR DEM 9(c). These errors may be attributed to both the visible floodwater extent extraction errors and the absolute errors between the CDEM and the LiDAR DEM. Different from previous research on floodwater depth mapping which evaluates absolute depth accuracy with the same flood extent polygons (Cohen et al., 2022), the flood extent predictions will be different when using different DEMs. Moreover, given the limited resources, ground-truth flood depth maps produced by a high-quality hydraulic model is not available. As the profile lines compared in Fig. 5, the absolute differences between the CDEM and the LiDAR DEM are much larger than the scale of the reconstructed elevation details by the proposed DEM upscaling method, adding the differences in floodwater extent estimation, a quantitative flood depth evaluation is not sensible due to the limitations of DEMs. The estimated floodwater depth map produced by the proposed method could be used in emergency response as a more effective reference compared to depth maps produced by LR DEMs.

4. Discussions and limitations

The production of accurate near-real-time flood maps during disaster response scenarios requires both accurate HR DEM and accurate visible floodwater extent extraction. This research attempted to utilize deep learning methods to produce the two critical components with the DEM upsampling network and the floodwater extraction network in the proposed framework. This attempt is intended for a proof of concept with basic CNN network structures applied, and implementing more advanced networks, such as vision transformers (Dosovitskiy et al., 2021), would likely further improve the results. As shown in Figs. 8 and 9, the proposed framework has shown significant improvement over manual processing of the aerial optical imagery and the flood mapping with the LR CDEM in the 2013 Calgary flood mapping, but there are still some limitations and areas for improvement in these two processes.

4.1. DEM upscaling

The proposed DEM upscaling network is specifically designed for urban areas with limited vegetation canopy coverage to reconstruct urban features for floodwater mapping. This proposed method only

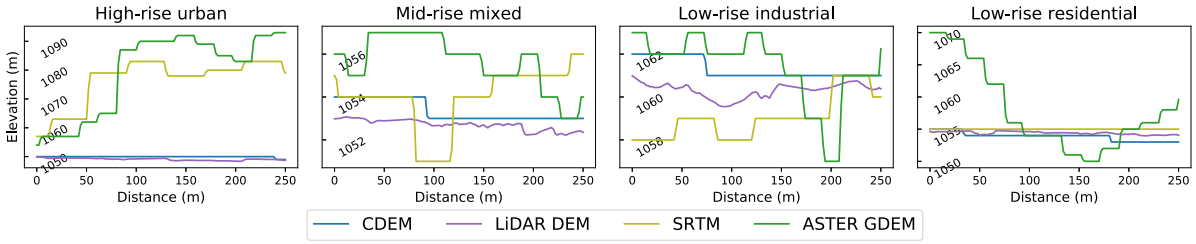

Fig. 10. Comparison of profiles of different DEM products.

adds urban topographical details, such as roads and building footprints, inferred from HR optical images, and the base DEM itself is not involved in the network, so the quality of flood maps produced by the proposed flood mapping workflow heavily relies on the accuracy and precision of the DEM products. As the results in Table 2 showed that DEMs with lower spatial resolutions may be more sensitive to visible floodwater extraction errors. The accuracy of floodwater extent and depth mapping also relies on the absolute elevation accuracy or the relative accuracy of flood-related topographic features. As shown in Fig. 5, the proposed DEM upsampling method can reconstruct urban topographic details from HR optical imagery and add it to the base DEM to better support flood mapping purposes. However, this method does not fix errors and uncertainties in the base LR DEMs. In this study, the low elevation precision of 1 m in CDEM may lead to abrupt elevation changes in the upscaled DEMs as shown in Fig. 5. Cohen et al. (2022) pointed out that the acquisition and processing quality of DEMs could be more important than spatial resolution in generating accurate flood depth estimation. Fig. 10 compares two common global DEM products, Shuttle Radar Topography Mission (SRTM) 1 arc-second DEM, and ASTER Global DEM (GDEM), together with CDEM and the LiDAR DEM in the same profile lines as the samples in Fig. 5. The CDEM has a spatial resolution of approximately 18 m, while SRTM and ASTER GDEM have a spatial resolution of approximately 30 m. Compared with the LiDAR DEM produced in 2012, ignoring the data collection time differences, the LR DEMs do have significant elevation errors, making them difficult to delineate HR urban flood mapping results. Among these DEMs, CDEM has the most consistent and reliable result, with errors usually within 2 m, even though it is the oldest product collected before the 1990s. The SRTM and ASTER GDEM have similar error rates to CDEM in low-rise urban environments but very large errors of over 20 m in high-rise urban environments. Therefore, the DEM products either by radar interferometry or digital photogrammetry do not provide reliable results in high-density urban regions. As a result, even though the LR CDEM is outdated, it can still reliably represent the underlying terrain surface in Canadian urban regions, so improved HR flood maps could be produced by the proposed DEM upsampling method with support from HR optical imagery.

There are also some limitations of the proposed DEM upscaling method that need to be addressed to make it more generalized to achieve a broader range of applicability. First, the proposed DEM upscaling network is specifically designed for urban areas with limited vegetation canopy coverage to reconstruct urban features for floodwater mapping, so that road networks and building footprints are the main HR features that the method intends to extract from the HR optical images. Meanwhile, optical images with thick vegetation coverage or dense high-rise buildings do not provide enough relevant features for topographic reconstruction, so this method works best in low-to-mid-rise urban areas. As the results shown in Fig. 5, the improvements under high-rise buildings and thick vegetation are very limited due to the limitation of optical images. HR synthetic aperture radar (SAR) imagery could be an alternative in densely vegetated areas, but new solutions are needed to tackle high-rise urban areas. Second, the training data utilized in this research have spatial and temporal limitations. Spatially, the training data are all distributed in Southern Ontario, which may limit the spatial diversity in terrain, building, and vegetation types. The testing area, Calgary, AB, is far from the training area with over 15 km^2 of an urban area, which is much larger than some similar research that tests algorithms on small image patches. The convergence of the network means that some identifiable features such as roads and building footprints do hold some consistency across regions in Canada, showing cross-regional compatibility to some degree. The proposed DEM upscaling method may not be directly applied in other regions due to different building codes and infrastructure types, and constructing a DEM dataset covering different countries similar to OpenGF (Qin et al., 2023b) would increase the spatial adaptability. Temporally, the three selected datasets were all collected in early spring leaf-off seasons, and data augmentation techniques could not compensate for the lack of diversity of the vegetation canopy. The aerial imagery of Calgary in this study was taken in late September 2012, when leaves of deciduous trees had fallen, so some image features are closely related to the training set despite some differences in vegetation colours. To apply this method to an area with imagery taken in leaf-on season, a more diverse training set would be ideal for contributing to the robustness of this method. Finally, the resolution of the base DEM and the target upscaling resolution will limit the performance of the proposed method. The proposed process chose the CDEM product at 18 m resolution as the base DEM due to the high quality and availability of the CDEM in Canada, and any other Canadian urban regions without HR LiDAR DEMs or researchers studying historical events would greatly benefit from the outcomes of this research. Additionally, there could be pixel alignment problems during the upsampling and downsampling process (OpenDEM, 2021). This study chose the 9 (from 18 m to 2 m) as the scale of resampling during the training data preparation to minimize the alignment issue, but some errors caused by pixel alignment when applying the proposed DEM upscaling method could not be neglected to some extent. As a result, directly applying this method on base DEMs at a different resolution, in a different geographical region, or in a different season may not produce the best performance depending on the use case.

4.2. *Visible floodwater extraction*

The proposed visible floodwater extraction network took advantage of an existing open accessible HR flood dataset, FloodNet (Rahnemoonfar et al., 2021), to perform a transfer learning strategy in order to extract visible floodwater from the 2013 flood in Calgary successfully. However, FloodNet only covers HR optical images in one flood event, limiting the diversity of floodwater characteristics. With the emergence of more and more open datasets for disaster management, such as the SpaceNet-8 dataset (Hänsch et al., 2022), a more diversified training dataset for flood monitoring could be assembled to improve the performance of the proposed method. The FloodNet and SpaceNet-8 datasets mostly cover clear water floods, while the 2013 flood in Calgary is a fluvial flood with mostly turbid floodwater with a very different spectral signature in optical images. Due to the similarity in

the spectral response of all water bodies in the RGB aerial imagery used in this research, floodwater and permanent water bodies were not treated separately in the floodwater extraction process. Flood events with diversified floodwater types and permanent water bodies with different spectral characteristics would need more diversified training sample labelling to ensure the performance of the proposed method, and these complex flood events need to be further tested in future studies. Despite the difficulties of obtaining HR optical images during flood events due to weather reasons, the increasing availability of UAV sensors worldwide may contribute to the quantity and quality of flood images for the development of better flood mapping techniques.

The proposed visible floodwater mapping method takes 10% of the flooded image tiles from the aerial imagery and achieved over 80% IoU by adopting a transfer learning procedure. According to the quantitative results provided in Table 2, there are still a lot of room for improvement in accurate delineation of visible floodwater. The simple network structure and transfer learning procedure provide a viable solution for a quick preliminary result during disaster response, and higher accuracy in visible floodwater extraction could be obtained by adopting a more advanced neural network structure or training scheme. A very recent study by He et al. (2022) utilized a semi-supervised method to extract visible open floodwater as well as areas under building and vegetation shadows in the same study area, and over 90% IoU was achieved with 5% of the annotated tiles. Although only using a small proportion of the labelled training set could result in high accuracy in visible floodwater extent prediction, transfer learning or semi-supervised learning still require full pixel-wise annotation of floodwater to train the deep neural network. In real-world disaster response scenarios, despite flood experts may select higher-quality and higher-diversity data for detailed annotation, which could result in a better performance for this proposed method where random stratified sampling was adopted for demonstration purposes, it is often not realistic to accurately perform pixel-wise labelling. Therefore, applying weakly-supervised methods would be more practical in disaster response scenarios with limited resources (Bonafilia et al., 2020).

Last but not least, the extraction of visible floodwater extent is intended to estimate local flood elevation to guide the floodwater mapping tool to infer floodwater extent and depth from the HR DEM. Additional data sources, including water gauges, public cameras and social media, would help refine flood estimation from remote sensing images to achieve improved real-time flood monitoring (Huang et al., 2018). More advanced and hydraulic-incorporated inundation estimation models can also be introduced to correct errors in floodwater extent extraction from remote sensing imagery (Bryant et al., 2022).

5. Conclusions

This research proposed a novel multi-sensory urban flood mapping framework to enable rapid near-real-time HR urban flood mapping. The proposed framework addressed the limitation of the existing flood mapping methods that only consider the visible floodwater extent in optical images by utilizing an upscaled HR DEM. It utilizes a DEM upscaling procedure to fill the data gap in urban regions without HR DEMs by reconstructing urban topographic details from HR optical imagery. The proposed framework consists of three major components: (1) A new DEM upscaling network with deep learning and image fusion by taking existing HR RGB aerial imagery to reconstruct HR urban topographic details, (2) A rapid visible floodwater extent extraction semantic segmentation network with a transfer learning strategy that requires a minimal amount of human labelling, (3) An accurate floodwater extent and flood depth estimation tool built with GIS hydrology analysis that takes both the visible floodwater extent and the upscaled HR DEM.

Through the case study on the flood event in Calgary in 2013, where HR aerial imagery was taken during the peak of the flood event, it can be found that: (1) The proposed DEM upscaling method can reconstruct HR urban topography details from an HR RGB aerial optical imagery to enhance the existing LR CDEM at 18 m resolution into 2 m resolution DEM products to support flood mapping. (2) The proposed visible floodwater extraction method takes advantage of an open-source flood mapping dataset to accurately extract visible floodwater at over 80% IoU from the real-time VHR RGB aerial imagery with only labelling 10% of the area and about 10 min of training time. (3) The proposed GIS-based flood mapping tool predicted floodwater extent and flood depth estimation using the extracted visible floodwater extent and the upscaled DEM achieved significant improvement over estimations using the LR CDEM.

The proposed framework could benefit urban regions without HR LiDAR DEMs to better respond to potential future flood events or perform retrospective studies on historical flood events, and it can be applied in a large-scale urban setting effectively with limited manual processing. The case study conducted in this research is a proof-of-concept of the proposed framework to show the practicality of using real-world data, and extensive testing is still required to make it an operational tool for disaster response. Given that near-real-time HR flood images and corresponding HR DEMs are not often available, as more and more HR geospatial data are becoming publicly accessible, the proposed framework will be further tested in other major urban areas in Canada. The intention of this research is to propose a flood mapping framework with simple network structures to demonstrate the feasibility of the concept without relying on the complicated advanced neural network structures. Future research will address the several limitations in the process discussed in the previous section, and more advanced deep learning structures will be explored to improve the performance of the proposed framework.

CRediT authorship contribution statement

Weikai Tan: Conceptualization, Data curation, Formal analysis, Investigation, Methodology, Resources, Software, Validation, Visualization, Writing – original draft, Writing – review & editing. **Nannan Qin:** Funding acquisition, Methodology, Validation, Visualization, Writing – review & editing. **Ying Zhang:** Conceptualization, Data curation, Funding acquisition, Project administration, Resources, Supervision, Writing – review & editing. **Heather McGrath:** Writing – review & editing. **Maxim Fortin:** Writing – review & editing. **Jonathan Li:** Funding acquisition, Resources, Supervision, Writing – review & editing.

Declaration of competing interest

The authors declare that they have no known competing financial interests or personal relationships that could have appeared to influence the work reported in this paper.

Data availability

The authors do not have permission to share data.

Acknowledgements

This research was supported in part by Natural Resources Canada [research affiliate program number 1000462062] and the National Natural Science Foundation of China [grant number 42001400]. Thanks to Natural Resources Canada and the City of Calgary for providing the geospatial data required for this research.

References

Amirkolaee, H.A., Arefi, H., 2021. Generating a highly detailed DSM from a single high-resolution satellite image and an SRTM elevation model. Remote Sens. Lett. 12 (4), 335–344. http://dx.doi.org/10.1080/2150704X.2021.1880659.

Argudo, O., Chica, A., Andujar, C., 2018. Terrain super-resolution through aerial imagery and fully convolutional networks. Comput. Graph. Forum 37 (2), 101–110. http://dx.doi.org/10.1111/cgf.13345.

Bonafilia, D., Tellman, B., Anderson, T., Issenberg, E., 2020. Sen1Floods11: A georeferenced dataset to train and test deep learning flood algorithms for Sentinel-1. In: 2020 IEEE Comput. Soc. Conf. Comput. Vis. Pattern Recognit. Workshops (CVPRW). pp. 835–845. http://dx.doi.org/10.1109/CVPRW50498.2020.00113.

Bryant, S., McGrath, H., Boudreault, M., 2022. Gridded flood depth estimates from satellite-derived inundations. Nat. Hazards Earth Syst. Sci. 22 (4), 1437–1450. http://dx.doi.org/10.5194/nhess-22-1437-2022.

City of Calgary, 2021. Flooding in calgary - Flood of 2013. URL: https://www.calgary.ca/content/www/en/home/uep/water/flood-info/flooding-history-calgary.html, Accessed on 2021-11-22.

Casas, A., Benito, G., Thorndycraft, V.R., Rico, M., 2006. The topographic data source of digital terrain models as a key element in the accuracy of hydraulic flood modelling. Earth Surf. Process. Landf. 31 (4), 444–456. http://dx.doi.org/10.1002/esp.1278.

Chen, Z., Wang, X., Xu, Z., Hou, W., 2016. Convolutional neural network based DEM super resolution. Int. Arch. Photogramm. Remote Sens. Spatial Inf. Sci. XLI-B3, 247–250. http://dx.doi.org/10.5194/isprsarchives-XLI-B3-247-2016.

Chen, L.-C., Zhu, Y., Papandreou, G., Schroff, F., Adam, H., 2018. Encoder-decoder with atrous separable convolution for semantic image segmentation. In: Proc. Eur. Conf. Comput. Vis.. pp. 833–851. http://dx.doi.org/10.1007/978-3-030-01234-2_49.

Cian, F., Marconcini, M., Ceccato, P., Giupponi, C., 2018. Flood depth estimation by means of high-resolution SAR images and lidar data. Nat. Hazards Earth Syst. Sci. 18 (11), 3063–3084. http://dx.doi.org/10.5194/nhess-18-3063-2018.

Cohen, S., Brakenridge, G.R., Kettner, A., Bates, B., Nelson, J., McDonald, R., Huang, Y.-F., Munasinghe, D., Zhang, J., 2018. Estimating floodwater depths from flood inundation maps and topography. J. Am. Water Resour. Assoc. 54 (4), 847–858. http://dx.doi.org/10.1111/1752-1688.12609.

Cohen, S., Peter, B.G., Haag, A., Munasinghe, D., Moragoda, N., Narayanan, A., May, S., 2022. Sensitivity of remote sensing floodwater depth calculation to boundary filtering and digital elevation model selections. Remote Sens. 14 (21), 5313. http://dx.doi.org/10.3390/rs14215313.

Cohen, S., Raney, A., Munasinghe, D., Loftis, J.D., Molthan, A., Bell, J., Rogers, L., Galantowicz, J., Brakenridge, G.R., Kettner, A.J., Huang, Y.-F., Tsang, Y.-P., 2019. The floodwater depth estimation tool (FwDET v2.0) for improved remote sensing analysis of coastal flooding. Nat. Hazards Earth Syst. Sci. 19 (9), 2053–2065. http://dx.doi.org/10.5194/nhess-19-2053-2019.

de Almeida, G.A.M., Bates, P., Ozdemir, H., 2018. Modelling urban floods at submetre resolution: Challenges or opportunities for flood risk management? J. Flood Risk Manag. 11 (S2), S855–S865. http://dx.doi.org/10.1111/jfr3.12276.

Demiray, B.Z., Sit, M., Demir, I., 2021. D-SRGAN: DEM super-resolution with generative adversarial networks. SN Comput. Sci. 2 (1), 2–48. http://dx.doi.org/10.1007/s42979-020-00442-2.

Deng, J., Dong, W., Socher, R., Li, L.-J., Li, K., Fei-Fei, L., 2009. ImageNet: A large-scale hierarchical image database. In: 2009 IEEE Comput. Soc. Conf. Comput. Vis. Pattern Recognit. (CVPR). pp. 248–255. http://dx.doi.org/10.1109/CVPR.2009.5206848.

DeVries, B., Huang, C., Armston, J., Huang, W., Jones, J.W., Lang, M.W., 2020. Rapid and robust monitoring of flood events using Sentinel-1 and landsat data on the google earth engine. Remote Sens. Environ. 240, 111664. http://dx.doi.org/10.1016/j.rse.2020.111664.

Dosovitskiy, A., Beyer, L., Kolesnikov, A., Weissenborn, D., Zhai, X., Unterthiner, T., Dehghani, M., Minderer, M., Heigold, G., Gelly, S., Uszkoreit, J., Houlsby, N., 2021. An image is worth 16x16 words: transformers for image recognition at scale. In: Proc. Int. Conf. Learn. Represent. (ICLR) 2021. pp. 1–21.

Dottori, F., Baldassarre, G.D., Todini, E., 2013. Detailed data is welcome, but with a pinch of salt: Accuracy, precision, and uncertainty in flood inundation modeling. Water Resour. Res. 49 (9), 6079–6085. http://dx.doi.org/10.1002/wrcr.20406.

ESRI Inc, 2021. ArcGIS pro. URL: https://www.esri.com/en-us/arcgis/products/arcgis-pro/overview.

Feng, Q., Liu, J., Gong, J., 2015. Urban flood mapping based on unmanned aerial vehicle remote sensing and random forest classifier—A Case of yuyao, China. Water 7 (4), 1437–1455. http://dx.doi.org/10.3390/w7041437.

Fernandez-Beltran, R., Latorre-Carmona, P., Pla, F., 2017. Single-frame super-resolution in remote sensing: A practical overview. Int. J. Remote Sens. 38 (1), http://dx.doi.org/10.1080/01431161.2016.1264027.

Feyisa, G.L., Meilby, H., Fensholt, R., Proud, S.R., 2014. Automated water extraction index: A new technique for surface water mapping using landsat imagery. Remote Sens. Environ. 140, 23–35. http://dx.doi.org/10.1016/j.rse.2013.08.029.

Gebrehiwot, A.A., Hashemi-Beni, L., 2021. Three-dimensional inundation mapping using UAV image segmentation and digital surface model. ISPRS Int. J. Geo-Inf. 10 (3), 144. http://dx.doi.org/10.3390/ijgi10030144.

Gebrehiwot, A., Hashemi-Beni, L., Thompson, G., Kordjamshidi, P., Langan, T.E., 2019. Deep convolutional neural network for flood extent mapping using unmanned aerial vehicles data. Sensors 19 (7), 1486. http://dx.doi.org/10.3390/s19071486.

Gerl, T., Bochow, M., Kreibich, H., 2014. Flood damage modeling on the basis of urban structure mapping using high-resolution remote sensing data. Water 6 (8), 2367–2393. http://dx.doi.org/10.3390/w6082367.

Gyamfi, C., Ndambuki, J.M., Salim, R.W., 2016. Hydrological responses to land use/cover changes in the olifants basin, South Africa. Water 8 (12), 588. http://dx.doi.org/10.3390/w8120588.

Haile, A.T., Rientjes, T.H.M., 2005. Effects of LiDAR DEM Resolution in Flood Modelling: A Model Sensitivity Study for the City of Tegucigalpa, Honduras. ISPRS WG III/3, III/4 3, pp. 12–14.

Hänsch, R., Arndt, J., Lunga, D., Gibb, M., Pedelose, T., Boedihardjo, A., Petrie, D., Bacastow, T.M., 2022. SpaceNet 8 - The detection of flooded roads and buildings. In: 2022 IEEE Comput. Soc. Conf. Comput. Vis. Pattern Recognit. Workshops (CVPRW). pp. 1471–1479. http://dx.doi.org/10.1109/CVPRW56347.2022.00153.

Hashemi-Beni, L., Gebrehiwot, A.A., 2021. Flood extent mapping: An integrated method using deep learning and region growing using UAV optical data. IEEE J. Sel. Top. Appl. Earth Obs. Remote Sens. 14, 2127–2135. http://dx.doi.org/10.1109/JSTARS.2021.3051873.

He, Y., Wang, J., Zhang, Y., Liao, C., 2022. Enhancement of urban floodwater mapping from aerial imagery with dense shadows via semisupervised learning. IEEE J. Sel. Top. Appl. Earth Obs. Remote Sens. 15, 9086–9101. http://dx.doi.org/10.1109/JSTARS.2022.3215730.

He, K., Zhang, X., Ren, S., Sun, J., 2016. Deep residual learning for image recognition. In: 2016 IEEE Comput. Soc. Conf. Comput. Vis. Pattern Recognit. (CVPR). pp. 770–778. http://dx.doi.org/10.1109/CVPR.2016.90.

Huang, C., Chen, Y., Wu, J., Chen, Z., Li, L., Liu, R., Yu, J., 2014. Integration of remotely sensed inundation extent and high-precision topographic data for mapping inundation depth. In: 2014 Int. Conf. Agro-Geoinf.. pp. 1–4. http://dx.doi.org/10.1109/Agro-Geoinformatics.2014.6910580.

Huang, X., Wang, C., Li, Z., 2018. A near real-time flood-mapping approach by integrating social media and post-event satellite imagery. Ann. GIS 24 (2), 113–123. http://dx.doi.org/10.1080/19475683.2018.1450787.

IPCC, 2014. Summary for policymakers. In: Clim. Chang. 2014: Impacts, Adapt., and Vulnerability. Part a: Glob. and Sectoral Aspects. Contrib. of Working Group II To the Fifth Assess. Report of the Intergov. Panel on Clim. Chang.. pp. 1–32.

Jamali, B., Löwe, R., Bach, P.M., Urich, C., Arnbjerg-Nielsen, K., Deletic, A., 2018. A rapid urban flood inundation and damage assessment model. J. Hydrol. 564, 1085–1098. http://dx.doi.org/10.1016/j.jhydrol.2018.07.064.

Jhee, H., Cho, H.-C., Kahng, H.-K., Cheung, S., 2013. Multiscale quadtree model fusion with super-resolution for blocky artefact removal. Remote Sens. Lett. 4 (4), 325–334. http://dx.doi.org/10.1080/2150704X.2012.729869.

Joyce, K.E., Belliss, S.E., Samsonov, S.V., McNeill, S.J., Glassey, P.J., 2009. A review of the status of satellite remote sensing and image processing techniques for mapping natural hazards and disasters. PPG: Earth Environ. 33 (2), 183–207. http://dx.doi.org/10.1177/0309133309339563.

Kingma, D.P., Ba, J., 2015. Adam: A method for stochastic optimization. In: Proc. Int. Conf. Learn. Represent. ICLR 2015. pp. 1–13, URL: https://arxiv.org/abs/1412.6980.

Kubade, A., Patel, D., Sharma, A., Rajan, K.S., 2021. AFN: Attentional feedback network based 3D terrain super-resolution. In: Proc. Asian Conf. Comput. Vis. ACCV 2020, Vol. 12622. pp. 192–208. http://dx.doi.org/10.1007/978-3-030-69525-5_12.

Ma, F., Cavalheiro, G.V., Karaman, S., 2019. Self-supervised sparse-to-dense: Self-supervised depth completion from LiDAR and monocular camera. In: 2019 IEEE Int. Conf. Robot. Autom. (ICRA). pp. 3288–3295. http://dx.doi.org/10.1109/ICRA.2019.8793637.

Maksimović, Č., Prodanović, D., Boonya-Aroonnet, S., Leitão, J.P., Djordjević, S., Allitt, R., 2009. Overland flow and pathway analysis for modelling of urban pluvial flooding. J. Hydraul. Res. 47 (4), 512–523. http://dx.doi.org/10.1080/00221686.2009.9522027.

Mason, D.C., Speck, R., Devereux, B., Schumann, G.J., Neal, J.C., Bates, P.D., 2010. Flood detection in urban areas using TerraSAR-X. IEEE Trans. Geosci. Remote Sens. 48 (2), 882–894. http://dx.doi.org/10.1109/TGRS.2009.2029236.

McFeeters, S.K., 1996. The use of the Normalized Difference Water Index (NDWI) in the delineation of open water features. Int. J. Remote Sens. 17 (7), 1425–1432. http://dx.doi.org/10.1080/01431169608948714.

Meng, X., Shen, H., Li, H., Zhang, L., Fu, R., 2019. Review of the pansharpening methods for remote sensing images based on the idea of meta-analysis: Practical discussion and challenges. Inform. Fusion 46, 102–113. http://dx.doi.org/10.1016/j.inffus.2018.05.006.

Merz, B., Kreibich, H., Schwarze, R., Thieken, A., 2010. Review article "Assessment of economic flood damage". Nat. Hazards Earth Syst. Sci. 10 (8), 1697–1724. http://dx.doi.org/10.5194/nhess-10-1697-2010.

Mignot, E., Li, X., Dewals, B., 2019. Experimental modelling of urban flooding: A review. J. Hydrol. 568, 334–342. http://dx.doi.org/10.1016/j.jhydrol.2018.11.001.

MMSegmentation Contributors, 2020. MMSegmentation: OpenMMLab semantic segmentation toolbox and benchmark. URL: https://github.com/open-mmlab/mmsegmentation.

Mou, L., Zhu, X.X., 2018. IM2HEIGHT: Height estimation from single monocular imagery via fully residual convolutional-deconvolutional network. pp. 1–13, arXiv:1802.10249 [cs], http://dx.doi.org/10.48550/arXiv.1802.10249.

Mueller, N., Lewis, A., Roberts, D., Ring, S., Melrose, R., Sixsmith, J., Lymburner, L., McIntyre, A., Tan, P., Curnow, S., Ip, A., 2016. Water observations from space: Mapping surface water from 25 years of landsat imagery across Australia. Remote Sens. Environ. 174, 341–352. http://dx.doi.org/10.1016/j.rse.2015.11.003.

Muhadi, N.A., Abdullah, A.F., Bejo, S.K., Mahadi, M.R., Mijic, A., 2020. The use of LiDAR-derived DEM in flood applications: A review. Remote Sens. 12 (14), 2308. http://dx.doi.org/10.3390/rs12142308.

National Research Council, 2007. Elevation Data for Floodplain Mapping. National Academies Press.

Néelz, S., Pender, G., 2010. Benchmarking of 2D hydraulic modelling packages. Technical Report, DEFRA/Environment Agency, UK, URL: https://assets.publishing.service.gov.uk/government/uploads/system/uploads/attachment_data/file/290884/scho0510bsno-e-e.pdf.

OMNRF, 2013. South Central Ontario Orthophotography Project (SCOOP) 2013. Ontario Ministry of Natural Resources and Forestry (OMNRF), URL: https://geohub.lio.gov.on.ca/documents/442deaef4b894470a57821a2b48f783e/about.

OMNRF, 2014. Digital Raster Acquisition Project Eastern Ontario (DRAPE) 2014. Ontario Ministry of Natural Resources and Forestry (OMNRF), URL: https://geohub.lio.gov.on.ca/documents/3f744636a8134155b0eeb037e4ee4367/about.

OMNRF, 2015. Southwestern Ontario Orthophotography Project (SWOOP) 2015. Ontario Ministry of Natural Resources and Forestry (OMNRF), URL: https://geohub.lio.gov.on.ca/documents/62d2c0ed59954290b35900b9e1fd8d44/about.

OpenDEM, 2021. Very Deep Super Resolution (VDSR) for improved resolution of digital elevation models. URL: https://www.opendem.info/superResolution.html.

Paszke, A., Gross, S., Massa, F., Lerer, A., Bradbury, J., Chanan, G., Killeen, T., Lin, Z., Gimelshein, N., Antiga, L., et al., 2019. Pytorch: An imperative style, high-performance deep learning library. Adv. Neural Inf. Process. Syst. 32, 1–12.

Peter, B.G., Cohen, S., Lucey, R., Munasinghe, D., Raney, A., Brakenridge, G.R., 2022. Google earth engine implementation of the floodwater depth estimation tool (FwDET-GEE) for rapid and large scale flood analysis. IEEE Geosci. Remote Sens. Lett. 19, 1–5. http://dx.doi.org/10.1109/LGRS.2020.3031190.

Qin, N., Tan, W., Guan, H., Wang, L., Ma, L., Tao, P., Fatholahi, S., Hu, X., Li, J., 2023a. Towards intelligent ground filtering of large-scale topographic point clouds: A comprehensive survey. Int. J. Appl. Earth Obs. Geoinf. 125, 103566.

Qin, N., Tan, W., Ma, L., Zhang, D., Guan, H., Li, J., 2023b. Deep learning for filtering the ground from ALS point clouds: A dataset, evaluations and issues. ISPRS J. Photogramm. Remote Sens. 202, 246–261. http://dx.doi.org/10.1016/j.isprsjprs.2023.06.005.

Rahnemoonfar, M., Chowdhury, T., Sarkar, A., Varshney, D., Yari, M., Murphy, R.R., 2021. FloodNet: A high resolution aerial imagery dataset for post flood scene understanding. IEEE Access 9, 89644–89654. http://dx.doi.org/10.1109/ACCESS.2021.3090981.

Ronneberger, O., Fischer, P., Brox, T., 2015. U-Net: Convolutional networks for biomedical image segmentation. In: Proc. Med. Image Comput. and Computer-Assisted Intervent. (MICCAI) 2015. pp. 234–241. http://dx.doi.org/10.1007/978-3-319-24574-4_28.

Shen, L., Li, C., 2010. Water body extraction from Landsat ETM+ imagery using adaboost algorithm. In: 2010 Int. Conf. Geoinf.. pp. 1–4. http://dx.doi.org/10.1109/GEOINFORMATICS.2010.5567762.

Tanguy, M., Chokmani, K., Bernier, M., Poulin, J., Raymond, S., 2017. River flood mapping in urban areas combining Radarsat-2 data and flood return period data. Remote Sens. Environ. 198, 442–459. http://dx.doi.org/10.1016/j.rse.2017.06.042.

Teng, J., Jakeman, A.J., Vaze, J., Croke, B.F.W., Dutta, D., Kim, S., 2017. Flood inundation modelling: A review of methods, recent advances and uncertainty analysis. Environ. Model. Softw. 90, 201–216. http://dx.doi.org/10.1016/j.envsoft.2017.01.006.

Wang, Z., Chen, J., Hoi, S.C., 2021. Deep learning for image super-resolution: A survey. IEEE Trans. Pattern Anal. Mach. Intell. 43 (10), 3365–3387. http://dx.doi.org/10.1109/TPAMI.2020.2982166.

Warren, I., Bach, H., 1992. MIKE 21: A modelling system for estuaries, coastal waters and seas. Environ. Softw. 7 (4), 229–240. http://dx.doi.org/10.1016/0266-9838(92)90006-P.

Webster, T.L., Forbes, D.L., MacKinnon, E., Roberts, D., 2006. Flood-risk mapping for storm-surge events and sea-level rise using lidar for southeast New Brunswick. Can. J. Remote Sens. 32 (2), 194–211. http://dx.doi.org/10.5589/m06-016.

Wu, Z., Zhao, Z., Ma, P., Huang, B., 2021. Real-world DEM super-resolution based on generative adversarial networks for improving InSAR topographic phase simulation. IEEE J. Sel. Top. Appl. Earth Obs. Remote Sens. 14, 8373–8385. http://dx.doi.org/10.1109/JSTARS.2021.3105123.

Xu, H., 2006. Modification of normalised difference water index (NDWI) to enhance open water features in remotely sensed imagery. Int. J. Remote Sens. 27 (14), 3025–3033. http://dx.doi.org/10.1080/01431160600589179.

Xu, Z., Chen, Z., Yi, W., Gui, Q., Hou, W., Ding, M., 2019. Deep gradient prior network for DEM super-resolution: Transfer learning from image to DEM. ISPRS J. Photogramm. Remote Sens. 150, 80–90. http://dx.doi.org/10.1016/j.isprsjprs.2019.02.008.

Xu, Z., Wang, X., Chen, Z., Xiong, D., Ding, M., Hou, W., 2015. Nonlocal similarity based DEM super resolution. ISPRS J. Photogramm. Remote Sens. 110, 48–54. http://dx.doi.org/10.1016/j.isprsjprs.2015.10.009.

Yue, L., Shen, H., Li, J., Yuan, Q., Zhang, H., Zhang, L., 2016. Image super-resolution: The techniques, applications, and future. Signal Process. 128, 389–408. http://dx.doi.org/10.1016/j.sigpro.2016.05.002.

Yue, L., Shen, H., Yuan, Q., Zhang, L., 2015. Fusion of multi-scale DEMs using a regularized super-resolution method. Int. J. Geogr. Inf. Sci. 29 (12), 2095–2120. http://dx.doi.org/10.1080/13658816.2015.1063639.

Zhang, Y., Canisius, F., Zhen, C., Feng, B., Crawford, P., Huang, L., 2019. Effectiveness of aerial and ISERV-ISS RGB photos for real-time urban floodwater mapping: Case of calgary 2013 flood. J. Appl. Rem. Sens. 13 (04), 1. http://dx.doi.org/10.1117/1.JRS.13.044521.

Zhang, Y., Crawford, P., 2020. Automated extraction of visible floodwater in dense urban areas from RGB aerial photos. Remote Sens. 12 (14), 2198. http://dx.doi.org/10.3390/rs12142198.

Zhang, Y., Yu, W., 2022. Comparison of DEM super-resolution methods based on interpolation and neural networks. Sensors 22 (3), 745. http://dx.doi.org/10.3390/s22030745.

Zhou, B., Zhao, H., Puig, X., Xiao, T., Fidler, S., Barriuso, A., Torralba, A., 2019. Semantic understanding of scenes through the ADE20K dataset. Int. J. Comput. Vis. 127 (3), 302–321. http://dx.doi.org/10.1007/s11263-018-1140-0.